

How Inhibitory Circuits Govern Multiband Neuronal Oscillations

Jiatong Guo

Huazhong University of Science and Technology | jiatongguo@ucsb.edu | [Homepage](#)

(Supervisor: Zhuocheng Xiao, New York University Shanghai)

PREFACE

This research document serves not only as a record of my work on computational neuroscience in the field of neuronal oscillations during my stay at NYU Shanghai in the summer of 2024, but also as a Quick-Start-Guide for upcoming researchers who will continue exploring the mysteries of neuronal synchronization and oscillations based on my research efforts. I have to step away from this project due to my upcoming commitments at UCSB where I will spend my entire senior year, so I aim to make this document as detailed as possible, providing an accurate and efficient reference to help you get started quickly and avoid detours and mistakes I encountered. The document is organized as follows:

- **Section 1, INTRODUCTION**, covers the background, mechanisms and functions of neural synchronization and oscillation.
- **Section 2, NETWORK SETTINGS**, describes how I determined the parameter sets for the neural network, which consists of excitatory neurons and two types of inhibitory neurons.
- **Section 3, METHODS**, provides technical details on setting up the neural network and the method of plotting the corresponding results in MATLAB.
- **Section 4, RESULTS AND ANALYSIS**, presents the simulation results, where I attempted to conclude the relationship between biological details and network dynamics observed in the simulations.
- **Section 5, FUTURE RESEARCH**, outlines potential directions for further research in both software simulations and hardware implementations, drawing on my understanding of this project and the research experience I gained at both NYUSH and HUST.

The document concludes with **SUMMARY AND ACKNOWLEDGEMENT**, as well as **REFERENCES**.

I. INTRODUCTION

“Clocks tick, bridges and skyscrapers vibrate, neuronal networks oscillate. Are neuronal oscillations an inevitable by-product, similar to bridge vibrations, or an essential part of the brain’s design?” [Science’2004]

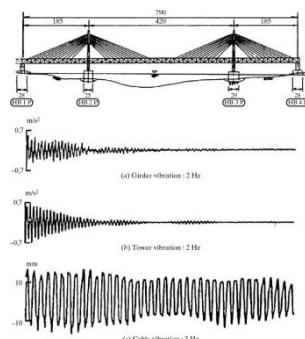


Fig. 1. Cable-stayed bridge vibration. [SEI’2013]

Neuronal oscillations are rhythmic patterns of electrical activity in the brain. Mammalian cortical neurons form behavior-dependent oscillating networks of various sizes, which span five orders of magnitude in frequency [Science’2004]. These oscillations are phylogenetically preserved, suggesting that they are functionally relevant. This project aims to uncover a systematic relationship between network’s biological details (e.g., synaptic strength) and the different types of neuronal oscillations (multiband oscillations) observed in the network dynamics when the local circuit is driven. In the future, we could make a systematic comparison between the numerical simulations results and the corresponding mathematical theory results, and even better, propose a new theory to interpret this kind of relationship.

A. Definition

1) ‘Neural’ or ‘Neuronal’

First of all, it’s necessary to clarify the concept difference between the term ‘neural’ and ‘neuronal’. The two terms are both related to the nervous system, but they have slightly different meanings and uses:

- **Neural**: Refers to anything related to the nervous system in general. It can describe functions, structures, processes, or fields of study involving the nervous system as a whole. For example: neural networks, neural activity, neural development. [Wiki]
- **Neuronal**: Specifically refers to neurons (the individual nerve cells). It is used in contexts that are directly related to the structure or function of neurons themselves. For example: neuronal connections, neuronal firing, neuronal structure.

Based on above statements and the fact that the focus of this project is the interplay between neurons and the connections within neurons, this document uses the term ‘neuronal’ more frequently.

2) Neuronal Synchronization and Oscillations

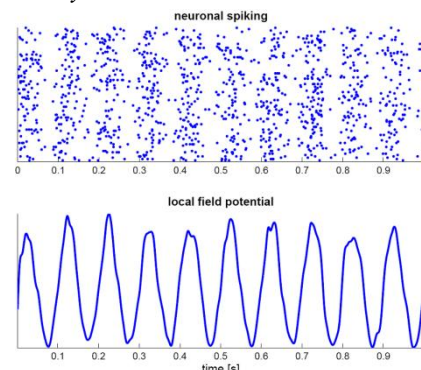
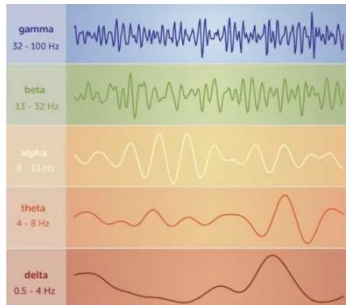


Fig. 2. Simulation of neuronal oscillation at 10 Hz. [Wiki]

Fig. 3. Frequency-based types of neuronal oscillation. [\[YouTube\]](#)

Neuronal synchronization refers to the phenomenon where two or more neurons fire action potentials in a coordinated manner, either at the same time or with a fixed timing relationship. This synchronization can occur at various scales, from local groups of neurons to larger networks across different brain regions.

Neuronal oscillation, as known as **brainwaves**, refers to rhythmic or repetitive patterns of electrical activity in neurons or neural circuits (Fig. 2), often characterized by a specific frequency (Fig. 3). For example, delta (0.1~4 Hz), theta (4~8 Hz), alpha (8~12 Hz), beta (12~30 Hz), gamma (30~100 Hz). Oscillations can be observed in individual neurons or across populations of neurons.

Neuronal synchronization and neuronal oscillation are closely related phenomena:

a) Oscillations as Synchronized Activity

Neuronal oscillations often reflect the synchronized firing of large groups of neurons. In this context, synchronization is a key driver of rhythmic oscillatory patterns. For example, gamma oscillations (30~80 Hz) often arise from synchronized interactions between excitatory pyramidal neurons and fast-spiking inhibitory interneurons (e.g., PV cells).

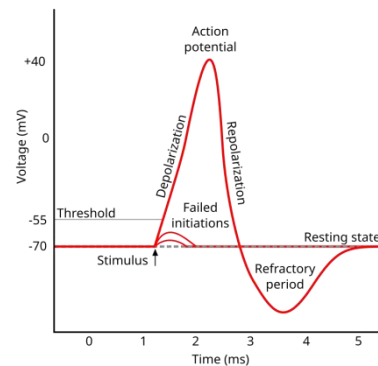
b) Synchronization Reinforces Oscillations

When neurons synchronize their firing, they can collectively produce oscillations with greater power and stability. The level of synchronization within a neural population can affect the strength and coherence of oscillations at specific frequencies.

c) Different Scales of Synchronization and Oscillation

Local synchronization among a small group of neurons can contribute to high-frequency oscillations (like gamma), while synchronization across larger populations of neurons over longer distances can support lower-frequency oscillations (like theta or delta). [\[Science'2004\]](#)

3) Important Terms

Fig. 4. Schematic of an action potential. [\[Wiki\]](#)

- **Excitatory neurons** are neurons that increase the likelihood of firing an action potential in their target cells by releasing excitatory neurotransmitters, such as glutamate, which typically depolarize the postsynaptic membrane.
- **Inhibitory interneurons** are neurons that decrease the likelihood of action potential generation in their target cells, usually by releasing inhibitory neurotransmitters like GABA, which hyperpolarize the postsynaptic membrane.
- **Projection probability** refers to the likelihood that one neuron forms a synaptic connection with another neuron, often described in probabilistic terms to represent the likelihood of connections in a neural network.
- **Synaptic strength** is the efficacy or magnitude of the synaptic transmission between two neurons, typically measured by the amplitude of the postsynaptic potential or current in response to a presynaptic action potential. In the context of my project where I used simplified and potential-normalized Integrate-and-Fire neuron model, the synaptic strength also denotes the value of the change of post-synaptic potential caused by one spike.
- **Time delay of dendritic inhibition**, in the context of this document, refers to the latency between the spike timing of an presynaptic inhibitory neuron, such as a somatostatin-expressing interneuron (SOM), and the timing when the resulting inhibitory signal starting affecting the membrane potential of the target neuron, which often influences the timing and integration of synaptic inputs. This time delay can reflect the fact that the dendrite of neurons is actually a tree instead of a point, and different target locations of presynaptic neurons will result in varying levels of time delay (see details in II.F) (Fig. 5).

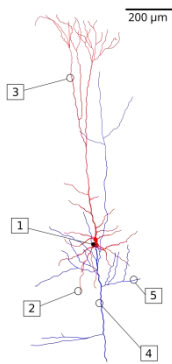


Fig. 5. Dendrite of a pyramidal neuron. Soma and dendrites are labeled in red, axon arbor in blue. (1) Soma, (2) Basal dendrite, (3) Apical dendrite, (4) Axon, (5) Collateral axon. [\[Wiki\]](#)

B. Mechanism behind Oscillations

Neuronal oscillations emerge from the balance and timing of excitatory and inhibitory signals within neural circuits. The oscillatory activity is often maintained through feedback loops, where excitatory neurons activate inhibitory neurons, which then suppress the excitatory neurons, creating a rhythmic cycle of excitation and inhibition. These feedback loops can occur at different frequencies depending on the properties of the neurons, the timescale of neural transmitters, the synaptic delays, and the network connectivity.

There is one strongly reduced heuristic theory behind neuronal oscillations proposed by [\[Annual Rev. Neuro.' 2009\]](#):

- Role of Interneurons:** Excitatory neurons drive the local network which includes basket cells (Fig. 6), a common type of interneuron.
- Synchronization through Inhibition:** The most strongly driven basket cell fires first, providing shunting inhibition to other basket cells. As this inhibition wears off synchronously, the basket cells will then fire roughly synchronously, entraining large numbers of basket cells to a rhythm after just a few of these cycles.
- Impact on Excitatory Neurons:** The rhythmically synchronized inhibition from basket cells impacts the local network's excitatory neurons, creating a short window for these neurons to fire when one bout of inhibition wears off and the next has not yet arrived.

The frequency of this kind of rhythm is primarily determined by the time constant of the shunting inhibition among basket cells.

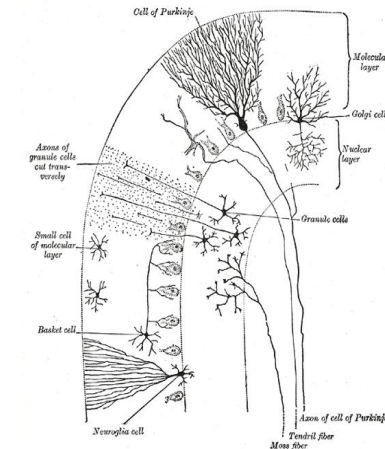


Fig. 6. Basket cell, a common type of interneuron that provides shunting inhibition onto each other and onto excitatory neurons. [\[Wiki\]](#)

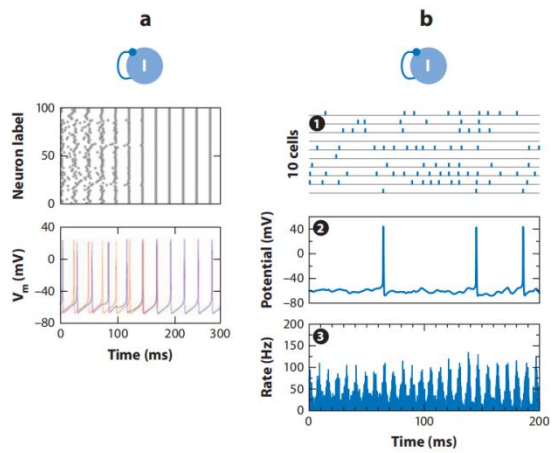


Fig. 7. Gamma oscillations in Inhibitory-Inhibitory model can emerge in two ways. (a) The input drive is relatively tonic, neurons can fire spike with a well-fined periodicity. (b) Neurons receive stochastic inputs (in noise-dominated regime) and fire spikes irregularly. [\[Annual Rev. Neuro.' 2012\]](#)

Two key mechanisms behind neuronal oscillations are Interneuron Network Gamma (ING) and Pyramidal-Interneuron Network Gamma (PING), which describe different types of network dynamics responsible for generating gamma-band oscillations (30-80 Hz).

1) ING: Interneuron Network Gamma

Interneuron Gamma (ING) oscillations occur when inhibitory interneurons, especially fast-spiking parvalbumin-positive (PV) interneurons, interact with each other without direct involvement from excitatory neurons. In ING, the oscillations are driven by inhibitory interneurons that form connections with each other via inhibitory synapses. Here's how it works:

- A subset of PV interneurons fires, inhibiting other nearby PV interneurons.
- After a brief refractory period, the inhibited interneurons recover and fire again.
- This cycle of inhibition and recovery generates synchronized oscillations, often at gamma frequencies (30-80 Hz).

Since ING is driven by inhibitory neurons alone, the frequency of the oscillation is primarily determined by the

synaptic delay and the refractory period of the inhibitory interneurons. ING tends to produce robust, high-frequency gamma oscillations.

A key ingredient of gamma oscillations is GABA (Gamma-AminoButyric Acid) receptor-mediated inhibition. Only three requirements are needed for Gamma oscillations to emerge:

- (1) A 'stripped-down' network model consisting only of mutually connected inhibitory interneurons.
- (2) A time constant provided by GABA receptors.
- (3) Sufficient drive to induce spiking in interneurons.

In both cases of **Fig. 7**, the emerging synchrony is caused when a subset of the interneurons begins to discharge together and generates synchronous inhibitory postsynaptic potentials in the partner neurons. [Annual Rev. Neuro. '2012]

2) PING: Pyramidal-Interneuron Network Gamma

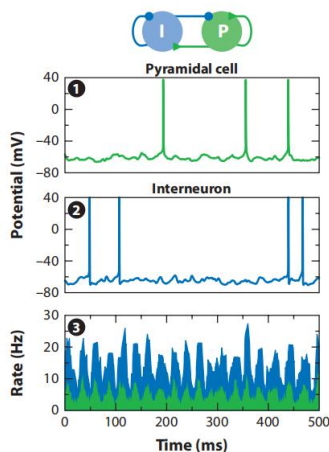


Fig. 8. Excitatory-Inhibitory model in gamma oscillations. [Annual Rev. Neuro. '2012]

Pyramidal-Interneuron Gamma (PING) oscillations involve the interaction between excitatory pyramidal neurons and inhibitory interneurons, creating a feedback loop between excitation and inhibition. The mechanism behind PING is as follows:

- Pyramidal cells (excitatory neurons) fire, sending excitatory signals to both other pyramidal cells and inhibitory interneurons (such as PV cells).
- In response, the inhibitory interneurons fire, which inhibits the pyramidal cells.
- Once the inhibition subsides, the pyramidal cells are ready to fire again, restarting the cycle.

PING is a relatively older model which posits gamma oscillations result from the reciprocal connections between pools of excitatory pyramidal neurons (E) and inhibitory interneurons (I), shown in **Fig. 8**. It has some key features:

- (1) Fast excitation from pyramidal cells to interneurons is often followed by a delayed feedback inhibition.
- (2) Appropriate strength of excitation and inhibition can allow for the persistence of cyclic behavior.
- (3) The phase shift between the pyramidal and interneuron spikes is often due to axon conduction

and synaptic delays, which can influence the frequency of the gamma rhythm.

In this case, the frequency of the oscillation is influenced by both the excitatory drive from pyramidal neurons and the inhibitory feedback from interneurons. PING can generate oscillations in a wide range of frequencies, but it is often associated with gamma oscillations, where the fast spiking of interneurons and the return of excitatory activity create rapid oscillatory cycles. Meanwhile, if a slow inhibitory source is present in the network, the oscillatory frequency will significantly decrease, as will be demonstrated later in this document.

To sum up, ING oscillations are generated by inhibitory interneurons interacting with each other, without direct excitatory input, which often creates fast gamma rhythms based on the timing of inhibition and recovery. PING oscillations arise from the interplay between excitatory pyramidal neurons and inhibitory interneurons, creating a feedback loop that alternates between excitation and inhibition, generating rhythmic activity at gamma frequencies.

Both ING and PING are important for neural synchronization and are critical for processes like attention and sensory processing, particularly in cortical circuits where gamma oscillations are prevalent.

C. Functions (Importance) of Neuronal Oscillations

Neuronal oscillations play a crucial role in coordinating and organizing neural activity across different brain regions. Their importance can be summarized in the following key functions [Science '2004]:

- (1) **Temporal Coordination:** Neuronal oscillations provide a timing mechanism that helps synchronize the activity of neurons across different brain regions. This synchronization allows for effective communication and information transfer between different parts of the brain, supporting cognitive processes like perception, memory, and attention.
- (2) **Communication Between Brain Regions:** Oscillations at similar frequencies across brain regions enable distant neurons to interact efficiently. This process, known as "communication through coherence," (**Fig. 9**) allows brain regions to become functionally connected by synchronizing their oscillatory activity.
- (3) **Segregation of Information:** Different frequency bands of oscillations can support different types of information processing. For example, slower oscillations (like theta) may handle long-range communication, while faster oscillations (like gamma) are more suited for local processing. This functional segregation allows the brain to process different streams of information simultaneously.
- (4) **Modulation of Synaptic Plasticity:** Oscillations, particularly those in the gamma and theta ranges, influence synaptic plasticity (the brain's ability to strengthen or weaken synapses based on activity). Oscillatory activity provides windows of opportunity for synaptic changes, supporting processes such as learning and memory formation.
- (5) **Input Selectivity:** Oscillatory activity helps neurons and networks respond selectively to inputs based on

their frequency characteristics. This frequency tuning allows for dynamic modulation of neuronal responsiveness, supporting processes like synaptic plasticity and information consolidation.

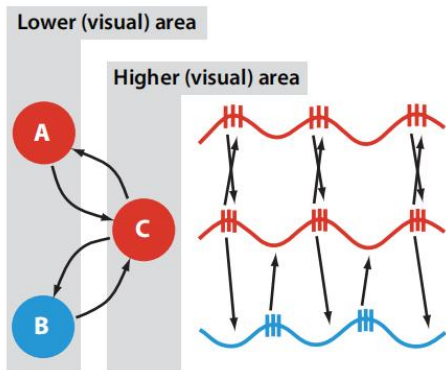


Fig. 9. The evidence for communication-through-coherence concept. Neuron group C is in-phase synchronized exclusively to A and not to B. [Annual Rev. Neuro.' 2009]

Besides above functions, neuronal oscillations also have relationship with attention and cognitive control, sensory processing and motor coordination, etc.

II. NETWORK SETTINGS

A. Different Neuron Types

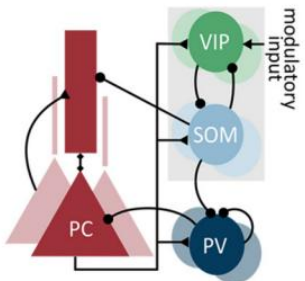


Fig. 10. The circuit model in [PLOS'2019].

In this project, I only consider four primary neuron types, which are Pyramidal Cells (PCs), Parvalbumin-positive interneurons (PVs), Somatostatin-positive interneurons (SOMs, also referred to as SSTs) and Vasoactive Intestinal Peptide-positive interneurons (VIPs). It has been proven that the three groups of interneurons account for nearly 100% of neocortical GABAergic neurons by [Dev. Neuro.'2011].

Here I summarized these four neuron types based on [Neuron'2016] in aspect of their functions, structure and connectivity:

(1) Pyramidal Cells (PCs) - Excitatory

- Function:** Pyramidal cells are the principal excitatory neurons in the cortex. They release glutamate, which depolarizes their target neurons, making them more likely to fire. Pyramidal cells are involved in various functions such as sensory perception, motor control, and cognitive processes like learning and memory.
- Structure:** These cells have a characteristic triangular-shaped soma, a long apical dendrite that extends towards the cortical surface, and several

basal dendrites (Fig. 5). Pyramidal cells are found throughout the neocortex and hippocampus.

- Connectivity:** They send excitatory signals to other excitatory and inhibitory neurons both locally within the same cortical area and to distant brain regions via long-range projections.

(2) Parvalbumin-positive Interneurons (PV) - Inhibitory

- Function:** PV interneurons provide fast, powerful inhibition to other neurons, especially pyramidal cells. They are critical for regulating the timing and synchronization of neuronal firing, particularly during high-frequency oscillations such as gamma rhythms (30-80 Hz), which are associated with cognitive functions like attention and working memory.
- Structure:** PV interneurons are fast-spiking cells and typically have basket or chandelier cell morphologies. Their perisomatic synapses primarily target the cell bodies and proximal dendrites of pyramidal cells, where they can effectively control neuronal output.
- Connectivity:** PV interneurons are connected to pyramidal neurons and other interneurons including, forming local inhibitory circuits that help synchronize network activity.

(3) Somatostatin-positive Interneurons (SOMs) - Inhibitory

- Function:** SOM interneurons provide dendritic inhibition to pyramidal neurons (and PV interneurons [Neuron'1996]), primarily targeting the distal dendrites. This type of inhibition regulates how pyramidal cells integrate synaptic inputs, especially excitatory signals coming from other cortical areas. SOM interneurons are also involved in modulating long-range cortical communication and top-down control during cognitive processes.
- Structure:** SOM neurons could be divided into three primary types [Nature Rev. Neuro' 2016]: Martinotti cells, which are defined by a multi-polar appearance and a prominent axonal arbor in L1; neurons with a bitufted appearance; and a small fraction of neurons that are characterized by a basket cell anatomy and fast-spiking phenotype. They, particularly Martinotti cells, extend axons that project to the upper layers of the cortex, often forming connections in layer 1. They play a key role in modulating the flow of information in cortical circuits.
- Connectivity:** SOM interneurons inhibit pyramidal neurons by suppressing inputs at their dendrites, thus controlling the integration of excitatory signals. They can also inhibit other types of interneurons (like PV basket cells), influencing the overall balance of excitation and inhibition in the network.

(4) Vasoactive Intestinal Peptide-positive Interneurons (VIP) - inhibitory

- Function:** VIP interneurons are involved in disinhibition, meaning they primarily inhibit other inhibitory interneurons, such as SOM neurons. By reducing the inhibitory influence of SOM neurons,

VIP cells can increase the excitability of pyramidal neurons. This disinhibitory mechanism is crucial during behaviors requiring heightened cortical activity, such as attention and learning.

2. **Structure:** VIP interneurons are often located in the superficial layers of the cortex and have a bipolar or multi-polar shape.
3. **Connectivity:** VIP interneurons primarily inhibit SOM interneurons, allowing pyramidal cells to receive less dendritic inhibition and become more excitable. They are typically activated by top-down inputs, such as during attention or task engagement, thus modulating cortical processing.

B. E/I Ratio

The E/I ratio (Excitation/Inhibition ratio) refers to the balance between excitatory and inhibitory activity in a neural network. It represents the proportion of excitatory input to inhibitory input that neurons receive. Maintaining an appropriate E/I ratio is crucial for the stability and functionality of neural circuits, as it regulates the overall level of network excitability, preventing runaway excitation or excessive inhibition.

In computational neuroscience, the E/I ratio is often set or adjusted during model calibration to match experimental data. It can be manipulated by changing the synaptic weights or projection probabilities of excitatory and inhibitory neurons. But first of all, we need to determine the ratio of excitatory to inhibitory neurons in a specific network or brain region. This ratio typically correlates with the overall E/I balance.

Given that this project aims to set up a small copy of mouse visual cortex L2/3, we should keep the ratio of excitatory and inhibitory neurons consistent with the experimental data. Here, I take the Allen Institute data as my reference ([Fig. 11](#)).

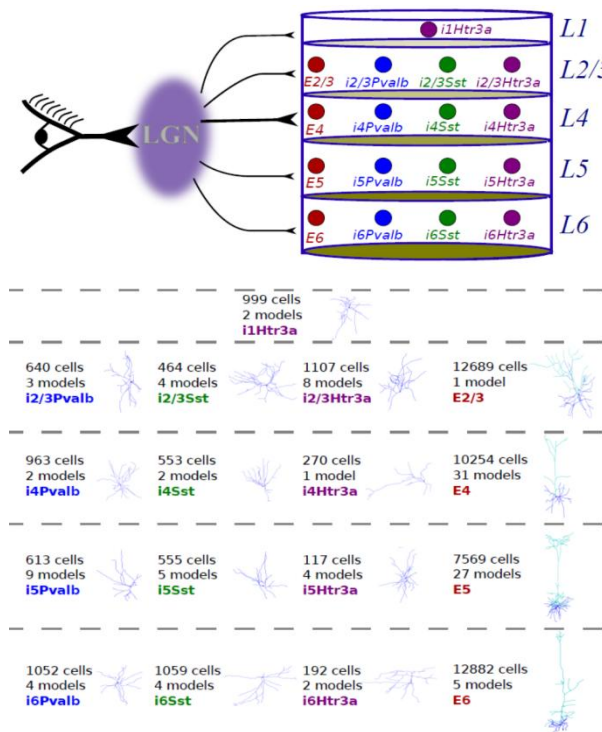


[Fig. 11. Models of the Mouse Primary Visual Cortex](#), from the Allen Institute [[Neuron'2020](#)], where LGN denotes Lateral Geniculate Nucleus, and Htr3a is a subclass of VIP interneurons.

C. Network Architecture

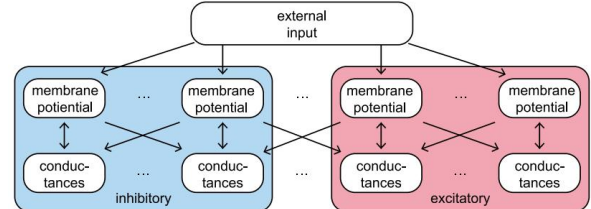


[Fig. 12. The Integrate-and-Fire network architecture](#) from [[Chaos'2023](#)].

In the beginning, I adopted the network architecture from [[Chaos'2023](#)], where they employ 300 excitatory neurons and 100 inhibitory interneurons both driven by constant input ([Fig. 12](#)). Interestingly, they find multiband oscillations emerging from this simple network by only adjusting one parameter: S_{ei} (synaptic strength from inhibitory interneuron to excitatory neurons). Based on their network, I first introduced SOM interneurons into the network to explore the network dynamics when there is another slow inhibition source presented.

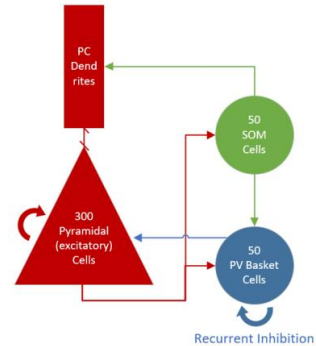


[Fig. 13. My network architecture - version 1](#).

[Fig. 13](#) presents the first version network architecture I used, where there are 300 PCs, 50 PVs and 50 SOMs. Compare to the network of [[Chaos'2023](#)], the only change I made is to replace 50 PVs with 50 SOMs (I don't consider VIP interneurons at initial stage). There are two things to note about: (1) SOM interneurons target the dendrites of pyramidal neurons instead of directly targeting their somas, which means we need to introduce some other parameter(s) to reflect this effect. (2) Unlike PV basket cells, SOM interneurons do not have recurrent inhibition within their own populations.

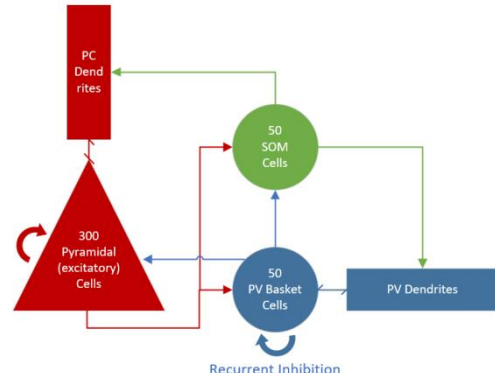


[Fig. 14. My network architecture - version 2](#).

As the project progresses, I got some new and important information, and made two updates to the network:

- (1) SOM interneurons also target the dendrites of PV basket cells, according to:

"The subcellular location of synapses from SST neurons on to other inhibitory cell types is an important variable in understanding their influence. For example, the proportion of SST-cell synapses on to PV neurons is more than twofold higher among their distal dendrites than on the somatic compartment." [Nature Rev. Neuro' 2016]

- (2) There exist projections from PV basket cells to SOM cells, and Allen Institute does provide the probability data of this kind of projection, though chances are that this projection data is actually caused by gap junction between these two types of neuron.

Here I summarized the input sources of each neuron type:

- (1) PC: excitation from other PCs + dendritic inhibition from SOMs + somatic inhibition from PVs
- (2) PV: excitation from PCs + dendritic inhibition from SOMs + recurrent inhibition from other PVs
- (3) SOM: excitation from PCs + inhibition from VIPs
- (4) VIP: excitation from PCs + inhibition from SOMs (+ external modulatory input)

In the late stage of this project, I tried to build up a small copy of Allen Institute's models of the mouse visual cortex L2/3, where there are 12689 Pyramidal cells, 640 PVs, 464 SOMs and 1107 VIP interneurons. The network's projection setting is in line with Fig. 14, while I used 1000 neurons (850 PCs + 75 PVs + 75 SOMs) and still didn't consider VIP neurons. The details of this network will be explained later in this document.

D. Projection Probability

Before we get down to the probability of projections (connections), we need to know that there are two totally different types of 'projection'.

One is the Erdős - Rényi (ER) model, in which all possible synaptic couplings are independently selected with probability P, excluding self-couplings. Once generated, the network connections are fixed and remained unchanged during simulation. Namely, the spikes of one neuron are only sent to its postsynaptic neurons.

The other is the 'annealed' architecture, where there are no real connections between neurons. When one neuron fires, all other neurons have the same probability P to receive the spike independently. Namely, the recipients of one specific neuron vary from spike to spike. In this case, the same-type neuron with the same membrane potentials are interchangeable.

I employed the ER model in my network. For large connection probability, the statistics of ER network dynamics are close to those of the annealed architecture. [Chaos'2023]

In [Chaos'2023], they set the probability of each type of projection as 0.8, which means a neuron has an 80% probability of forming a connection with another neuron. This '0.8' serves no actual physiological purpose because in

this paper they keep $P_{ij} * S_{ij}$ constant ($S_{ij,\text{normalized}} = S_{ij,\text{real}} / P_{ij}$, S denotes synaptic strength and P denotes projection probability) to ensure that the total post-synaptic potentials caused by one spike remain unchanged across the network, and thus make projection probability unimportant. So they just focus on adjusting synaptic strength, which makes some sense because synapses will undergo plastic process and modify their strength.

TABLE I. PROJECTION PROBABILITY AT AN INTERSOMATIC DISTANCE OF 75 MICROMETERS [NEURON'2020]

Trg Src	i1Htr3a	E2/3	i2/3 Pvalb	i2/3 Sst	i2/3 Htr3a
i1Htr3a	0.656	0.356	0.093	0.068	0.464
E2/3	0	0.16	0.395	0.182	0.105
i2/3Pva	0.024	0.411	0.451	0.03	0.22
i2/3Sst	0.279	0.424	0.857	0.082	0.77
i2/3Htr	0	0.087	0.02	0.625	0.028

At initial stage, I kept not looking into the projection probability and simply set them as 0.8, just like what [Chaos'2023] did in their paper, to test some parameter sets. In the later stage, I adopt the projection data directly from the Allen Institute [Neuron'2020] and conducted further parameter scanning.

However, I didn't realize this direct adoption is inappropriate until later in this project. The reason is, for one thing, the projection probability in their network is modeled as a Poisson distribution and varies from neurons to neurons, instead of remain the same in one type of projection in my network. For another, the network in Allen Institute is much more complex and contains much more information than ours, we need to think twice before we directly adopt any data from them without making any changes. If we want to make a small copy of their network, what really matters is the average number of neurons of each type that are targeting one specific neuron! Unfortunately, the Allen Institute paper [Neuron'2020] doesn't provide any information about this, so I proposed a model to roughly estimate this kind of data (the model still needs adjustment).

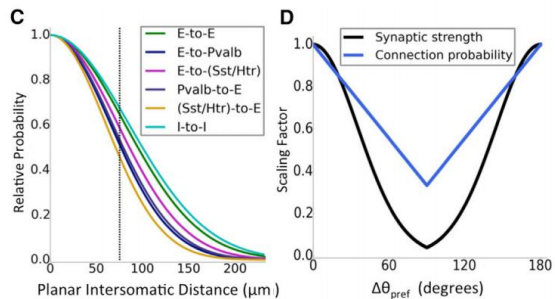


Fig. 15. The distance-dependent factor (left) and preferred-angle-dependent factor (right) of projection probability. [Neuron'2020]

Firstly, let's look into the details of projection probability in Allen Institute. They assume the projection probability is associated with two factors: distance-dependent factor and preferred-angle-dependent factor (Fig. 15).

$$P_{\text{src} \rightarrow \text{trg}} = P_{\text{dist}}(r) * P_{\text{angle}}(\Delta\theta) \quad (1)$$

Where r denotes distance and $\Delta\phi$ denotes angle difference.

$$P_{\text{dist}}(r) = A * e^{-\frac{r^2}{\sigma^2}} \quad (2)$$

The integral of this probability (2) from 0 to $R_0 = 75 \mu\text{m}$, divided by the area within the radius R_0 , should be equal to the reported measured probability (P_{rep}).

$$\frac{1}{\pi R_0^2} \oint A e^{-\frac{r^2}{\sigma^2}} dx dy = P_{\text{rep}} \quad (3)$$

The formula (3) establishes the relationship between the values reported in the **TABLE I** and our distance-dependent formula for connection probability :

$$A = \frac{P_{\text{rep}}}{\frac{\sigma^2}{R_0^2} \left(1 - e^{-\frac{R_0^2}{\sigma^2}} \right)} \quad (4)$$

From work in the mouse cortex [**J Neuro. 2012**], the standard deviations σ are estimated to be:

$$\sigma_{E \rightarrow E} = 114 \mu\text{m}$$

$$\sigma_{E \rightarrow PV} = 92 \mu\text{m}$$

$$\sigma_{E \rightarrow SOM} = 103 \mu\text{m}$$

$$\sigma_{SOM \rightarrow E} = 85 \mu\text{m}$$

$$\sigma_{PV \rightarrow E} = 95 \mu\text{m}$$

$$\sigma_{PV \rightarrow PV} = 120 \mu\text{m}$$

And they also assume that the connections among all inhibitory classes have the same distance dependence standard deviation.

$$P_{\text{angle}}(\Delta\phi) = B_1 + G\Delta\phi \quad (5)$$

With regard to the preferred-angle dependence, the Allen Institute assumes the dependence is linear (**Figure. 15. right**) as a function of the direction tuning difference ($\Delta\phi$), the difference of preferred angles of any two cells can be compressed to $[0^\circ, 90^\circ]$. For this model, the intercept occurs at $(0^\circ, B_1)$, and the other extreme of the model is $(90^\circ, B_2)$. The relative strength of the dependence can be described by a ratio $Q = B_2/B_1$. As can be seen, for like-to-like connection, $Q < 1$ (i.e., $G < 0$). Because $B_2 = Q*B_1$, the gradient can be expressed as:

$$G = \frac{Q*B_1 - B_1}{90^\circ - 0^\circ} = \frac{B_1(Q-1)}{90^\circ} \quad (6)$$

Integral of $P_{\text{src} \rightarrow \text{trg}}(\Delta\phi)$ (with normalization for the angle range) should be set to 1 to determine the scaling factor:

$$\frac{1}{90^\circ} \int_{0^\circ}^{90^\circ} (B_1 + G\Delta\phi) d\Delta\phi = 1 \quad (7)$$

And thus

$$B_2 = \frac{2Q}{1+Q} \quad (8)$$

The value of Q for Layer 2/3, 4, and 6 was set to 0.5 given the high direction selectivity. For Layer 5, it was set at

0.8 for the excitatory-to-excitatory connections due to lower direction selectivity in this layer.

Next I will introduce the model I proposed to roughly estimate the average number of connections of one specific neuron in mouse visual cortex L2/3. First of all, I made some assumptions:

- (1) Suppose the neurons nearby are evenly distributed.
- (2) In the network, there are 85% E-cells + 15% I-cells (4.3% PV, 3.1% SOM, 7.6% VIP). [**Neuron'2020**]
- (3) Only consider neurons within 200 μm , because the projection probability beyond 200 μm can be regarded as zero.
- (4) Introduce the distance scaling factor S_{dist} , to facilitate computing neurons in the distance range of [75, 200] μm .

$$S_{\text{dist}} = \frac{\text{Integral}_{75 \sim 200 \mu\text{m}}}{\text{Integral}_{0 \sim 75 \mu\text{m}}} \quad (9)$$

where Integral denotes the integral value of the Gaussian function (**Figure. 15. left**). I computed these values by the code file *Gaussian.m* shared in my Github. I summarized the results here:

TABLE II. THE DISTANCE SCALING FACTOR IN MY MODEL

Value	Type	$E \rightarrow E$	$E \rightarrow PV$	$E \rightarrow S^a$	$PV \rightarrow E$	$S \rightarrow E$	$I \rightarrow I$
	$\sigma (\mu\text{m})$	114	92	103	95	85	120
Scaling Factor	0.881	0.658	0.777	0.692	0.577	0.932	

^a S denotes SOM interneurons.

- (5) Introduce angle-preference scaling factor S_{angle}

$$S_{\text{angle}} = \frac{\text{Integral}_{0 \sim 90^\circ}}{\text{Rectangle}_{0 \sim 90^\circ}} \quad (10)$$

where Integral denotes the integral value of the function shown in (**Figure. 15. right**) and Rectangle denote the rectangular area. I consider the value of S_{angle} as a constant 0.65.

Then comes the formula:

$$N_{0 \sim 200 \mu\text{m}} = P * S_{\text{angle}} * (N_{0 \sim 75 \mu\text{m}} + N_{75 \sim 200 \mu\text{m}} * S_{\text{dist}}) \quad (11)$$

where N denotes the number of neurons, P denotes the projection probability and here I used the value of P from P_{rep} in **TABLE I**.

In mouse visual cortex L2/3, the value of cell density is 140000 per mm^3 [**Shuz & Palm'1989**], the median layer thickness is 210 μm [**Brain Atlas**], and thus the total cells in L2/3 core area with a radius of 0.4mm are 14778 neurons.

$$N_{0 \sim 75 \mu\text{m}} = \text{Cell Density} * \text{Volume}_{0 \sim 75 \mu\text{m}} = 274.4$$

$$N_{75 \sim 200 \mu\text{m}} = \text{Cell Density} * \text{Volume}_{75 \sim 200 \mu\text{m}} = 4444.0$$

Then we can compute the result for the average number of connections of one specific neuron in mouse V1 L2/3 using this estimation model.

TABLE III. THE AVERAGE NUMBER OF CONNECTIONS OF ONE SPECIFIC NEURON IN MOUSE VISUAL CORTEX L2/3, BASED ON ALLEN INSTITUTE DATA, ESTIMATED FROM MY MODEL.

Src	Trg	E-cells	PV	SOM	VIP
E-cells	E-cells	367.97	692.15	372.09	214.67
PV	PV	38.17	55.33	3.68	26.99
SOM	SOM	24.02	75.80	7.25	68.10
VIP	VIP	1.39	0.47	14.79	0.66

Prof. Xiao pointed out that the first row data are too big to be biologically realistic, so this estimation model still needs further improvement.

E. Synaptic Strength

Compared to the biologically realistic projection probability, the synaptic strength in the network is more fault-tolerant, because there is socalled ‘synaptic plasticity’. We can tune the synaptic strength to find out the network dynamics we want to explore. For example, the strengths of cortical synaptic couplings are: $S_{ee} = 0.0094$, $S_{ii} = 0.00245$, $S_{ie} = 0.0125$ and $S_{ei} = 0.00255$. They found out that different-beat rhythms are related with different S_{ei} (0.0245 for 1-beat rhythm and 0.0261 for 2-beat rhythm [**Chaos’2023**]).

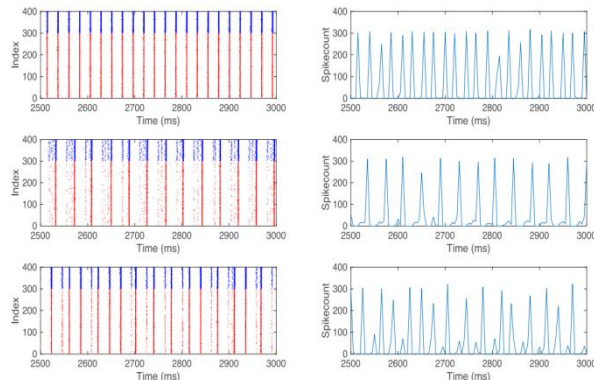


Fig. 16. Raster plots and spike count plots (in 5-ms windows) for E neurons exhibiting three different distinct rhythms of MFEs (Multiple-Firing Events) : 1-(up), 2-(mid), 3-(down) beat. [**Chaos’2023**]

In my network, I chose to use the synaptic strength data from Allen Institute as the starting point and gradually tuned them to explore the network dynamics (see details in IV).

The first version of Allen Institute V1 model used an orientation-dependent like-to-like rule for synaptic weights of all connection classes. Since neurons had pre-assigned preferred angles, the connection strength was a function of the difference between the assigned angles of two connected neurons, defined within 90° :

$$W = A_w e^{-\left(\frac{\Delta\theta}{\sigma_w}\right)^2} \quad (12)$$

where $\Delta\theta$ denotes the difference of assigned angles, σ_w denotes the standard deviation set to 50° for all connection type and A_w denotes the weight constant to be determined for each connection type to be matched to PSP (post-synaptic potentials) targets. Then Allen Institute adopted Grid Search Method to iteratively adjusted the synaptic weights in order to satisfy three criteria:

- (1) To match spontaneous firing rates to experimental observations.
- (2) To match peak firing rates for the drifting grating.
- (3) To avoid epileptic-like activity where the network would ramp up to have large global bursts and then enter a period of silence until the next very rapid burst.

For more details about the synaptic strength in Allen Institute, readers are recommended to read the *Methods* part of [**Neuron’2020**] as reference. All in all, we just need an appropriate starting point to begin our tuning for the synaptic strength.

Another thing we need to notice about is, before we use the synaptic strength data from Allen Institute, we need to check out whether these data apply to the neuron model in our network. Allen Institute use a Generalized Leaky-Integrate-and-Fire neuron model they developed themselves [**Nature Comm.’2018**], while the neuron model in my network is Simplified Integrate-and-Fire model [**Chaos’2023**] which I normalize the membrane potential by setting the resting potential (-70mV) as 0 and the threshold potential (-50mV) as 1. So I normalized the synaptic strength data in Allen Institute by means of dividing each of them by $(V_{\text{threshold}} - V_{\text{rest}})$.

TABLE IV. STRENGTH OF CONNECTIONS (SOMATIC UNITARY POST-SYNAPTIC POTENTIAL). [**NEURON’2020, FIG. 4B**]

Trg Src	i1Htr3a	E2/3	i2/3 Pvalb	i2/3 Sst	i2/3 Htr3a
i1Htr3a	1.73	0.53	0.48	0.57	0.78
E2/3	0	0.36	1.49	0.86	1.31
i2/3Pva	0.37	0.48	0.68	0.42	0.41
i2/3Sst	0.47	0.31	0.5	0.15	0.52
i2/3Htr	0	0.28	0.18	0.32	0.37

TABLE V. STRENGTHS OF CONNECTIONS AFTER NORMALIZATION

Trg Src	E-cells	PVs	SOM	VIP
E-cells	0.0195 ^a	0.075	0.043	0.065
PVs	0.024	0.034	0.021	0.021
SOM	0.0155	0.025	0.075	0.026
VIP	0.014	0.009	0.016	0.019

^a. There is one tiny misreading error in Allen institute data, the value in [Hofer et. al, 2011] is actually 30mv.

F. Time Delay of Dendritic Inhibition

Only the soma of neurons are capable of generating action potential or spike, and the spike is going to be transmitted

to both sides of dendrites and axons. As above mentioned, due to the fact that the dendrite of a neuron is actually a tree instead of a point (Fig. 5) and that pre-synaptic neurons target the different locations of dendrites will incur different levels of dendritic time delay, we need to introduce some other parameters to reflect this effect.

Normally when people try to model a new compartmental model, they usually use multiple points to represent one neuron. For example you can have one point to represent the soma itself, some other points for the dendrite trees (each point stands for one segment on the dendrite tree) and another few points for the axons. Of course this method is more biologically realistic but costly. There is another useful alternative which is less realistic but much easier to implement, just simply introduce a time delay in the spikes released by the SOM interneurons when they are projecting to pyramidal cells. This kind of time delay aims to reflect that the spikes will first arrive on the dendrites and then they will take some time to be transmitted to the soma. I chose to use the latter method for simplicity, and I introduced two parameters τ_{es}^{delay} and τ_{is}^{delay} to represent the time delay of spikes from SOM interneurons to pyramidal neurons and PV basket cells, respectively.

Firstly, we need to find out an appropriate scanning range for these two parameters.

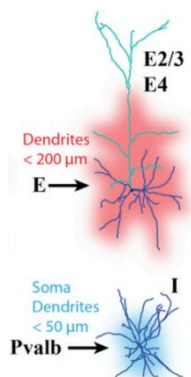


Fig. 17. Dendrites of pyramidal neurons and PV basket interneurons. [Neuron'2020]

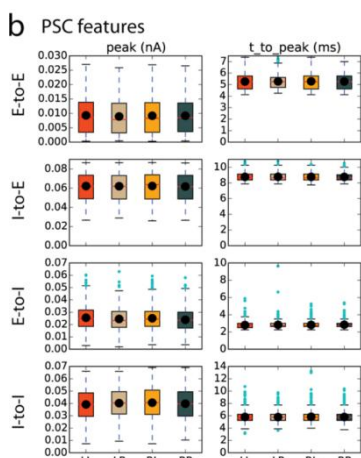


Fig. 18. Features of post-synaptic currents for the recurrent connections. [PLOS'2018]

According to [Neuron'1996], the dendritic IPSPs (Inhibitory Post-Synaptic Potentials) were slower than somatic IPSPs, with a time to peak (time between

presynaptic spike to the peak) of 7.6 ± 2.2 ms (somatic IPSPs: 2.8 ± 1.0 ms). And [Trends in Neurosciences'1997] reported that the velocity of action potentials in dendrites typically ranges from **0.05 to 0.5 m/s** depending on the type of neuron and the specific dendritic branch. Given that the typical dendrite length for pyramidal neurons is 200~500 μm and PV is 100~300μm, we can compute that the dendritic time delay ranges from 0.2~10ms, which corresponds to the results in [PLOS'2018] (Fig. 18). We can conclude that the range of **1~10 ms** is enough for us to scan the dendritic time delay parameters.

G. An Mental Challenge

What types of oscillatory dynamics could be produced by the disinhibitory circuit model shown in (Fig. 10) ?

As we know, each neuron has their own timescale in excitation and inhibition, and all of the oscillatory frequencies are the product of their interplay.

Given that the timescales for AMPA and GABA are 1~3ms and 4~6ms, the fast Gamma oscillations (30-80 Hz) are surely to be produced because of the presence of Pyramidal-Parvalbumin neurons loop.

In this network, the SOM interneurons introduce another type of timescale: dendritic time delay which ranges from 1 to 10 ms, so the Beta oscillations (12-30 Hz) should also be produced.

With regard to the slow oscillations - Alpha (8-12 Hz), Theta (4-8 Hz) and Delta (1-4 Hz) oscillations. We need to turn to another type of timescale which ranges from 30 to 200 ms caused by the Spike Frequency Adaptation (SFA) property of the SOM and VIP interneurons, which is another negative feedback mechanism besides recurrent inhibition. Readers are recommended to read about the SOM-VIP motif, which serves to translate weak signals onto VIP neurons into large changes of the somato-dendritic distribution of inhibition, in [PLOS'2019] for more details.

To sum up, theoretically, the disinhibitory circuit model shown in Fig.10 should be capable of producing neuronal oscillations of all of the frequency band.

III. METHODS

The code style of my network is in line with the code from [Chaos'2023], their code and scripts to produce all the figures in their paper can be found at : [\[Click here\]](#). My code and bare data are also available at [\[Click here\]](#).

A. Neuron Model

The current-based Integrate-and-Fire neuron model in my network is adapted from [Chaos'2023], in which the membrane potential v_i is driven toward V_{th} by the excitatory current and away from it through the inhibitory current. When the membrane potential v_i arrives at V_{th} , a spike is emitted by this neuron to all its postsynaptic cells, and v_i is immediately reset to the rest potential. After that, v_i is held at V_{rest} for an absolute refractory period.

Simplified version:

$$\frac{dv_i}{dt} = I_i^E + I_i^I. \quad (13)$$

Detailed Version:

$$\begin{aligned}
\frac{dv_i}{dt} &= (g_i^{\text{ext}} + g_i^E) \cdot (V_{\text{th}} - V_r) + g_i^I (V^I - v_i), \\
g_i^{\text{ext}} &= S_i^{\text{ext}} \sum_{\mu_i^{\text{ext}}} G^E \left(t - t_{\mu_i^{\text{ext}}} \right), \\
g_i^E &= \sum_{\substack{j \in E \\ j \neq i}} S_{ij}^E \sum_{\mu_j^E} G^E \left(t - t_{\mu_j^E} \right), \\
g_i^I &= \sum_{\substack{j \in I \\ j \neq i}} S_{ij}^I \sum_{\mu_j^I} G^I \left(t - t_{\mu_j^I} \right). \tag{14}
\end{aligned}$$

$$\begin{aligned}
G^E(t) &= \frac{1}{\tau^E} e^{-\frac{t}{\tau^E}} h(t), \\
G^I(t) &= \frac{1}{\tau^I} e^{-\frac{t}{\tau^I}} h(t),
\end{aligned}$$

The meanings of symbols in these formulas are as follows:

- i : neuron index
- v_i : normalized membrane potential (dimensionless)
- $I^{\{E, I\}}$: excitatory/inhibitory current
- V^E : excitatory reversal potential ($= 14/3$)
- V^I : inhibitory reversal potential ($= -2/3$)
- V_{th} : The spiking threshold potential ($= 1$)
- V_r : The rest membrane potential ($= 0$)
- τ_R : absolute refractory period ($= 0$ for simplicity)
- $g_i^{\{\text{ext}, E, I\}}$: external, excitatory, inhibitory conductance
- μ^{ext} : external stimulus
- $\mu^{\{E, I\}}$: recurrent E/I spikes series
- $S^{\{\text{ext}, E, I\}}$: the strengths of synaptic couplings
- $G(t)$: Green's functions for the E/I conductances
- $h(t)$: Heaviside function
- $\tau^{\{E, I\}}$: Timescales of synapses. (AMPA: $\tau^{EE}=1.4\text{ms}$, $\tau^{EI}=1.2\text{ms}$, GABA: $\tau^I=4.5\text{ms}$)

Note that the membrane potential in the model is normalized by setting the rest potential as 0 and threshold potential as 0.

In the code, the equation of the model is actually different:

$$\frac{dv_i}{dt} = (g_i^{\text{ext}} + g_i^E + g_i^I * \frac{v_i + M_r}{M + M_r}) * (V_{\text{th}} - V_{\text{rest}}) \tag{15}$$

$$S_{Q,I}(V_i) := (V_i + M_r)/(M + M_r) * S_{Q,I}. \tag{16}$$

Here, $S_{Q,I}$ denotes the size of jump of inhibitory synaptic strength at $v_i = M$. It is because when I-spike take effect, the rule is analogous to that of E-spikes, with the following exception: v_i jumps down instead of up by an amount proportional to $(v_i + M_r)$, where ' $-M_r$ ' is the reversal potential for I-currents, ' M ' is the spiking threshold. [J Math. Bio.'2019]

Tianyi Wu, a former student in Prof. Xiao's lab, said that they intentionally kept the equation unchanged in order to keep consistent with the Markov model in [J Math. Bio.'2019].

B. External Inputs

Normally there are two types of external inputs for one specific brain region. The first is Top-Down inputs, which originate from higher cortical areas and non-specific thalamocortical pathways. They selectively aim at apical dendrites and are thought to be associated with internal predictions. Another is Bottom-Up inputs, which come from lower cortical areas and the core thalamic nuclei. They primarily arrive at perisomatic regions and basal dendrites and are thought to carry information from the external world. Control of the different input streams, and consequently, information processing modes, is of fundamental importance [PLOS'2019].

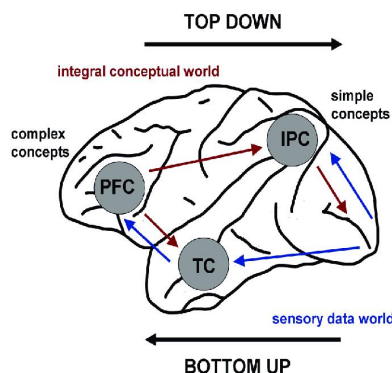


Fig. 19. Two types of input streams. [Sinke&Christopher'2013]

As for mouse visual cortex L2/3, it has three input sources:

- (1) Inputs from LGN (Lateral Geniculate Nucleus), which is a relay center in the thalamus that processes visual information and receives input from the retina and transmits this information to the primary visual cortex.
- (2) Inputs from other layers in the visual cortex.
- (3) Inputs from "Background Pool", the rest of the brain, which is modeled as a single input unit that fired at 1 kHz with a Poisson distribution. [Neuron'2020]

For simplicity, I only considered the inputs from the rest of the brain and didn't include any other input resources.

C. Network Building

In this part, I will briefly introduce the my codes about how to build a neural network on MATLAB. Readers are recommended to open the code files I shared above and then read this part.

The *eg-model-x.m* file is the top module, you can change the parameters and the parameter scanning settings in this file. The *model-LIF-SOM.m* is actually the code for the neural network.

In the beginning of this code, I first load the parameters and initialize the matrixes. The connections of the network are generated by Binornd funtion and stored in *connection_matrix*, in which 1 represents the corresponding two neurons are connected and 0 means there is no

connection between them. Remember to eliminate the self-connection.

Then the code generates the external Poisson input based on the external spike frequency parameters, these external inputs serve to make neurons fire at a realistic base-line rate.

After that the code enters Main Loop, where it first points out the neurons that are still in refractory period and then updates the membrane potential of active neurons. The following is the process for the effects of spikes. With regard to the dendritic inhibitions, I introduce some buffers. The buffers have rows of total delay steps and columns of target neurons. The first row stores the delayed SOM inhibition that arrives at soma from dendrites and the last row stores the newly produced SOM dendritic inhibition. In each simulation step, the first row of the buffer will be fetched out at input for the membrane potential update, and the buffer will then be updated to empty the last row for the incoming dendritic inhibition. The membrane potential of each neuron will be updated in each step, and the membrane potentials, the effects of spikes and spike count of each step will be stored in matrixes as outputs.

D. Output

As above mentioned, the output matrixes in my code contains the information below: the membrane potentials of each neuron in each step, the effects of spikes, and the timing and total amount of each spike for each neuron. Based on these data, we can draw raster plots to show the overall firings pattern of the network, and compute the correspond firing rate for each neuron type (see details in the file *rasterplot2.m*).

Moreover, it's more intuitional to analyze the network dynamics in the frequency-domain by applying Fourier Transform algorithm, and draw the Amplitude-Frequency plots, Energy Density plots and so on (see details in the file *fft-plot.m*).

IV. RESULTS AND ANALYSIS

In the first batches of simulation results shown in *Week4.pptx*, I tried to find out an appropriate data combination of projection probability and synaptic strength from **[Chaos'2023]** and **[Neuron'2020]**. However, if you zoom in the raster plots, you find tens of firing events in just one bar (**Fig. 20**), which is rather bizarre. Later I found out that there was still some errors in the code at that time, so the results here have little usefulness.

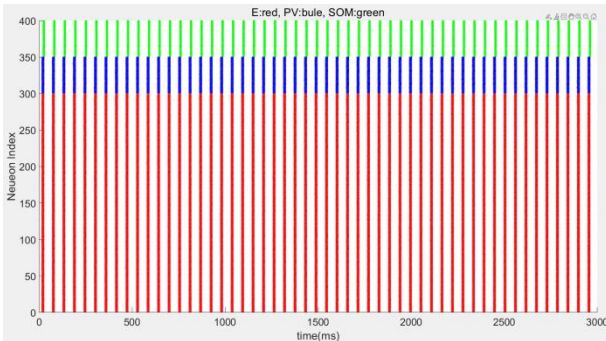
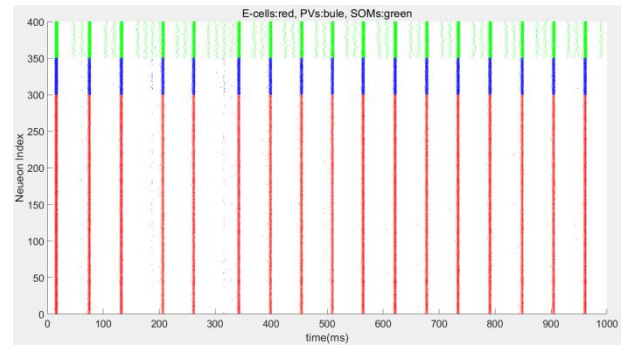


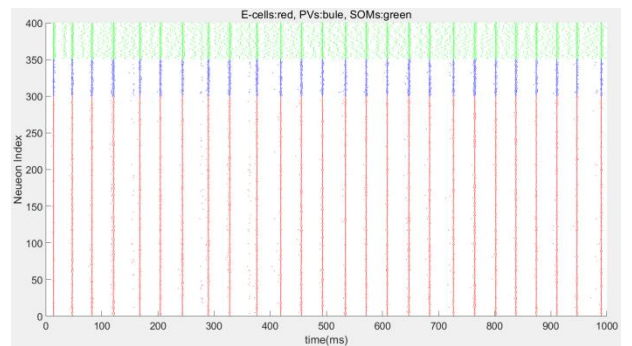
Fig. 20. Simulation result using projection probability and synaptic strength data from [Chaos'2023].

After I fixed the bugs in the code, I started scanning the parameters in the network. The first scanning object is the

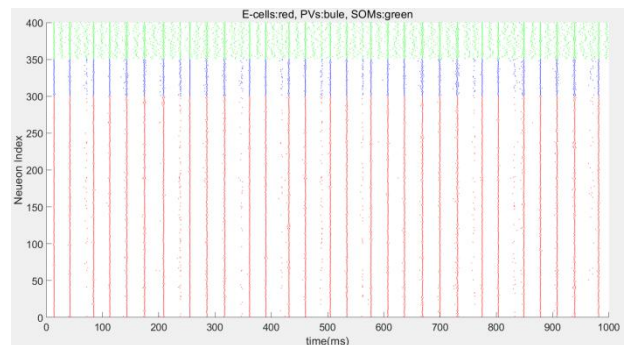
refractory period. I found that if refractory period equals zero, each neuron fires multiple times during one bar (as referred to as one Multi-Firing Event, MFE). And each neuron fires once or twice during one MFE if refractory period is not zero.



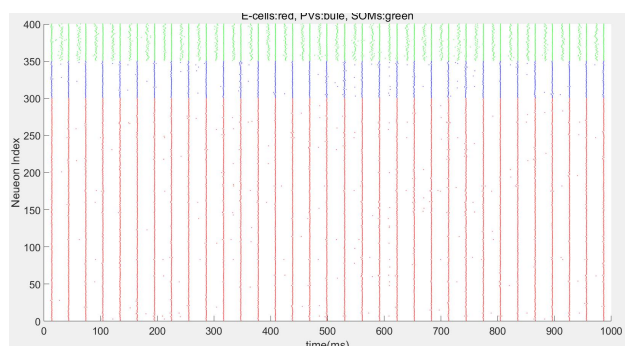
(a) Refractory period = 0, each neuron fires multiple times during one bar



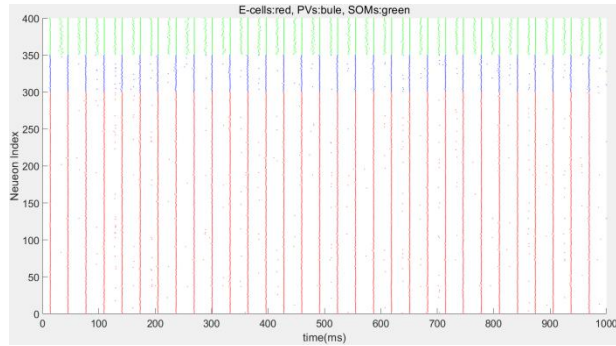
(b) Refractory period = 1ms.



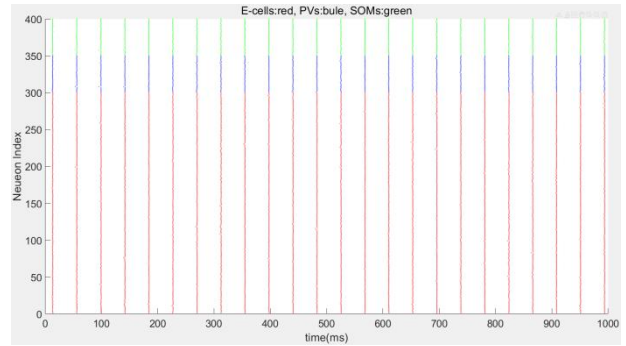
(c) Refractory period = 2ms.



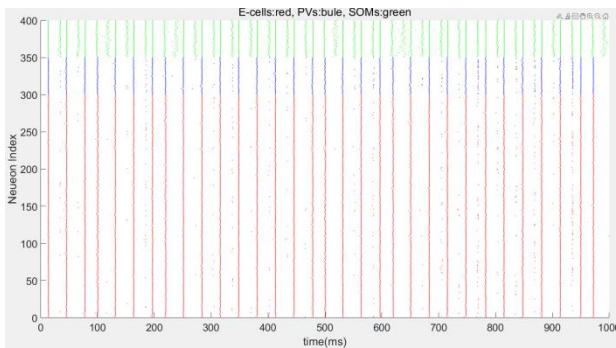
(d) Refractory period = 3ms.



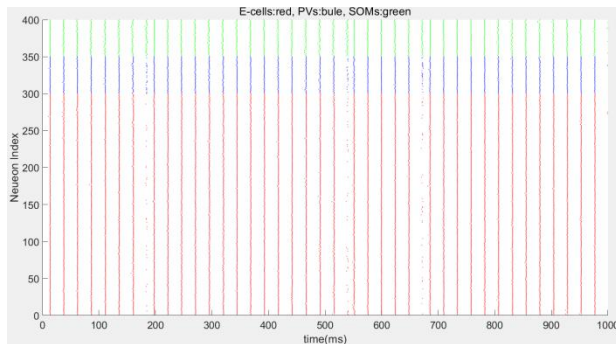
(e) Refractory period = 4ms.



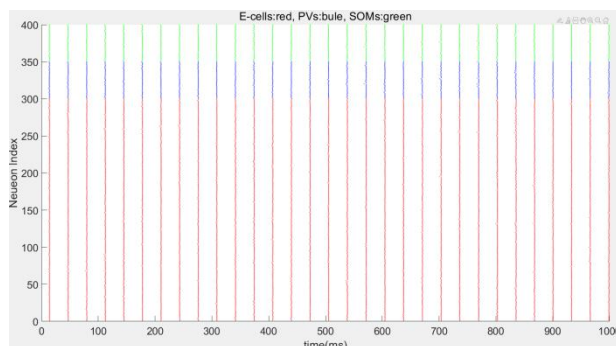
(i) Refractory period = 30ms.



(f) Refractory period = 5ms.



(g) Refractory period = 10ms.

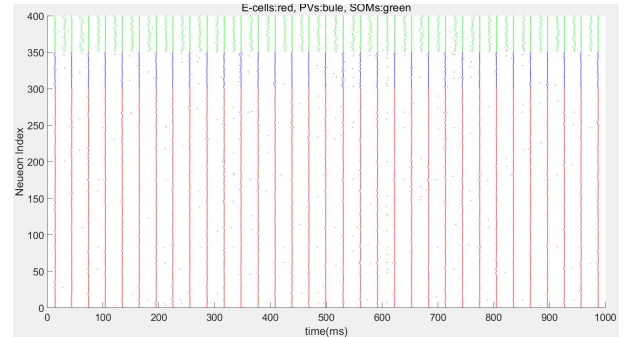
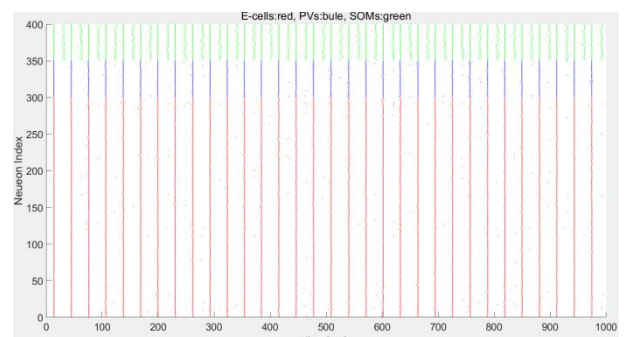


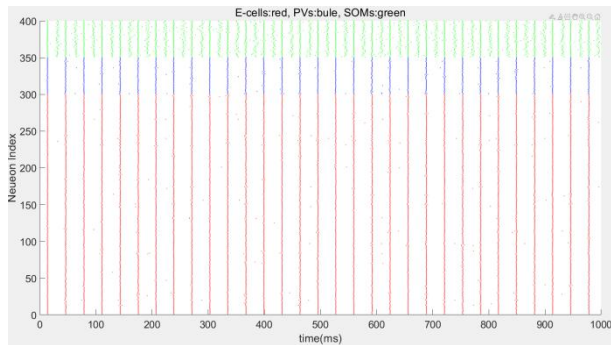
(h) Refractory period = 20ms.

Fig. 21. Simulation results with different values of refractory period. Both projection probability and synaptic strength data come from [Chaos'2023].

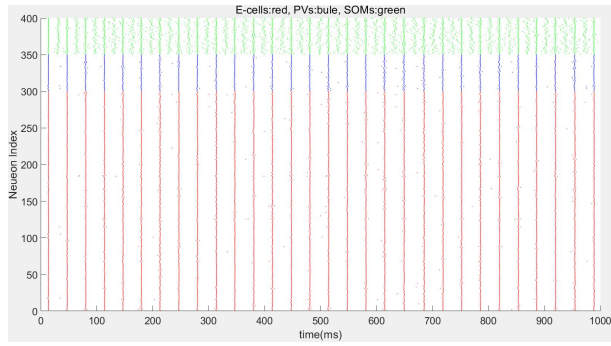
From above results we can see that there are already multiband oscillations, in some figures SOM interneurons fire at the middle-gamma band (about 60 Hz), while PCs and PVs fire at the low-gamma band (about 30 Hz). It should also be noted that when refractory period is large enough, the synchronization pattern is totally artificial (**Fig. 21. h&i**). Because in these cases, the interval of MFEs equal refractory period plus the base-line potential accumulating time caused by sole external input, which means the interplay between neurons is completely eliminated because of their long refractory period.

Then I scanned the time delay of dendritic inhibition from SOM interneurons, with the fixed value of refractory period (3 ms). Note that I used the same value for both τ_{es}^{delay} and τ_{is}^{delay} in the following simulations.

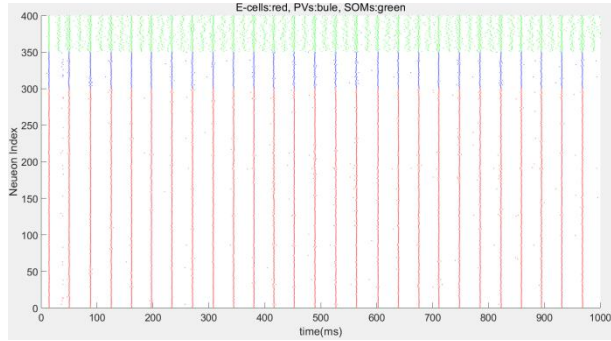

 (a) $\tau^{delay} = 1$ ms.

 (b) $\tau^{delay} = 2$ ms.



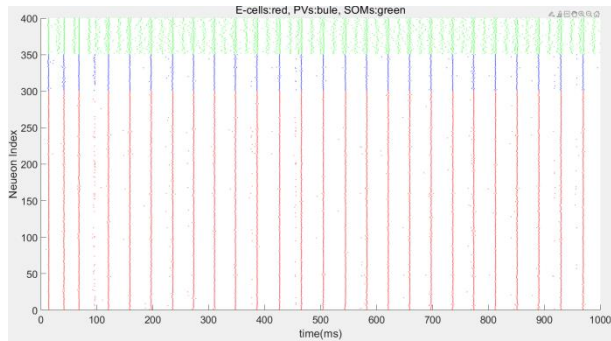
(c) $\tau^{delay} = 3\text{ms}$.



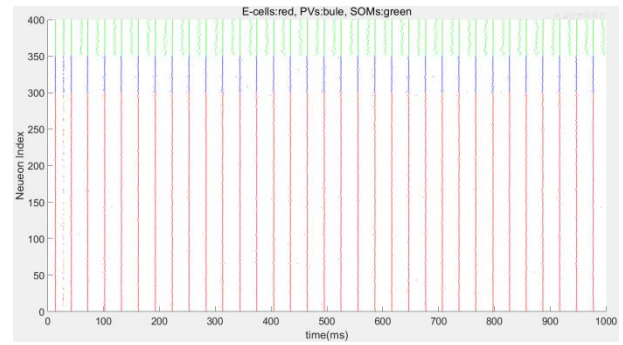
(d) $\tau^{delay} = 5\text{ms}$.



(e) $\tau^{delay} = 8\text{ms}$.



(f) $\tau^{delay} = 10\text{ms}$.



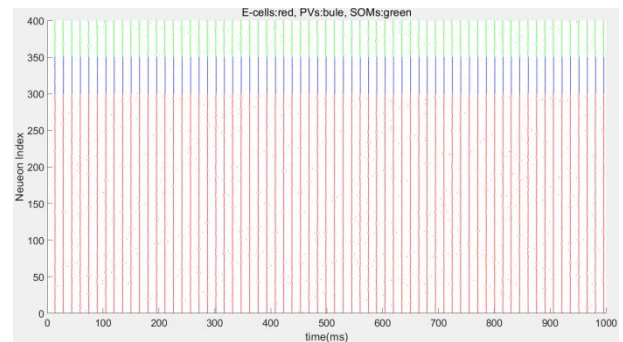
(g) $\tau^{delay} = 15\text{ms}$.

Fig. 22. Simulation results with different values of the time delay of dendritic inhibition from SOM interneurons. Both projection probability and synaptic strength data come from [Chaos' 2023].

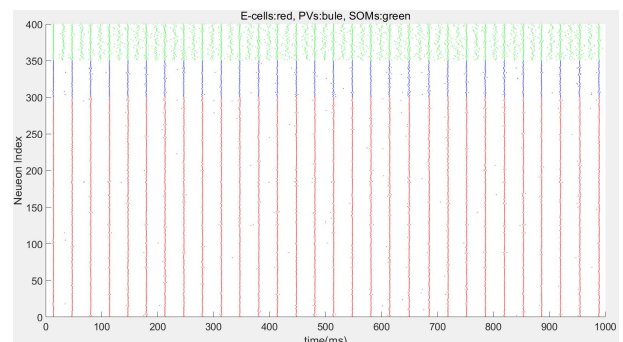
It can be summarized from above results that the firing rates of neurons gradually decline with the increasing value of the SOM time delay. PCs and PVs fire at a frequency from low-gamma band (about 33 Hz) to high-beta band (about 27 Hz). This phenomenon reflects that the oscillatory frequency of the neural network is largely influenced by the slower inhibition source, i.e., SOM interneurons.

Then I scanned the above two parameters (refractory period and SOM time delay) based on Allen Institute data set and also observed similar phenomena. You can find the detailed simulation results in *Week5.pptx*.

Next I swept the synaptic strength from SOM interneurons to pyramidal neurons (S_{es}) and PV interneurons (S_{is}) respectively, with the refractory period fixed at 3 ms and SOM time delay fixed at 5 ms. The simulation results is as follows.



(a) $S_{es} = 0.00$ (i.e. SOM interneurons are not involved in inhibiting PCs)



(b) $S_{es} = 0.0245$ (original data in [Chaos'2023])

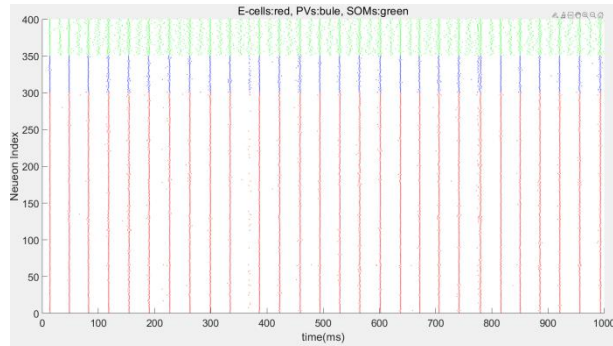
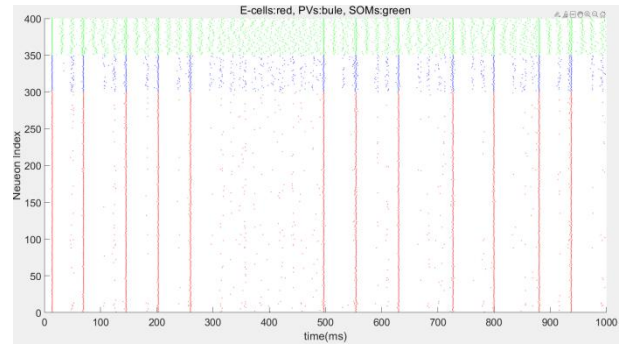
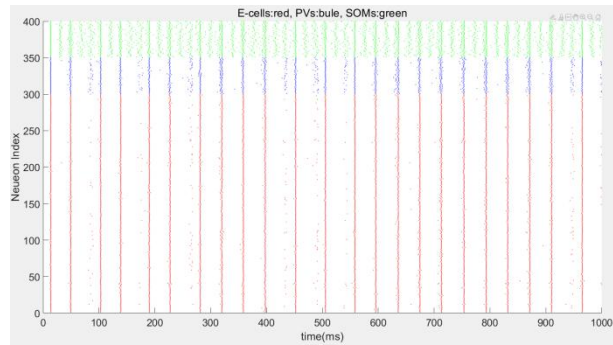
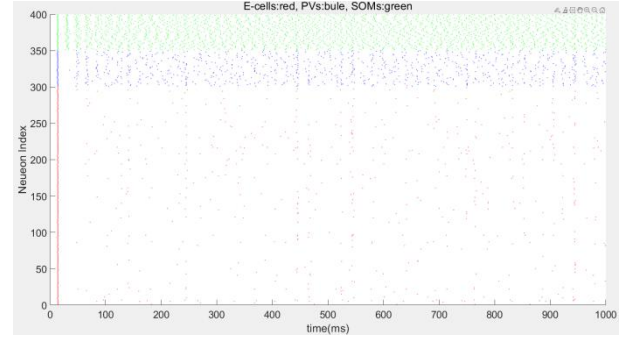
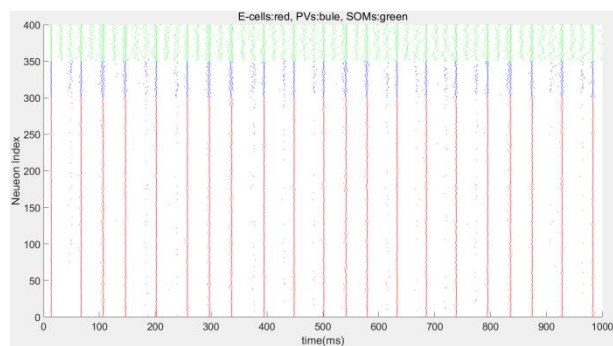
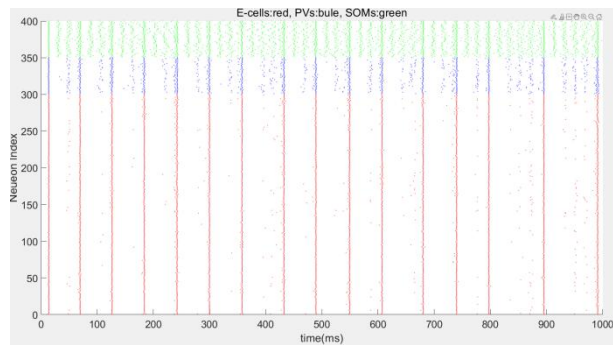
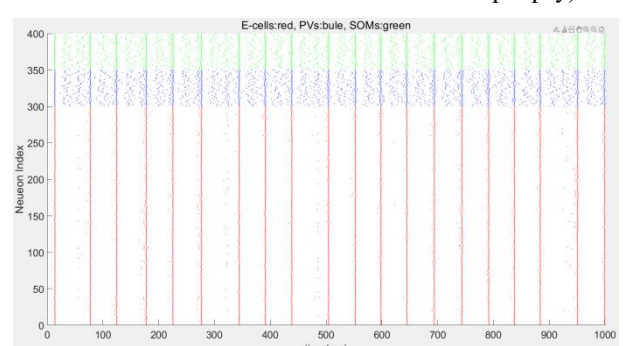
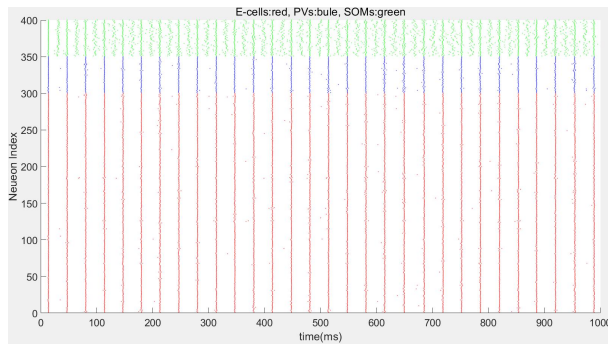

 (c) $S_{es} = 0.0258$

 (g) $S_{es} = 0.0307$

 (d) $S_{es} = 0.0270$

 (h) $S_{es} = 0.0319$

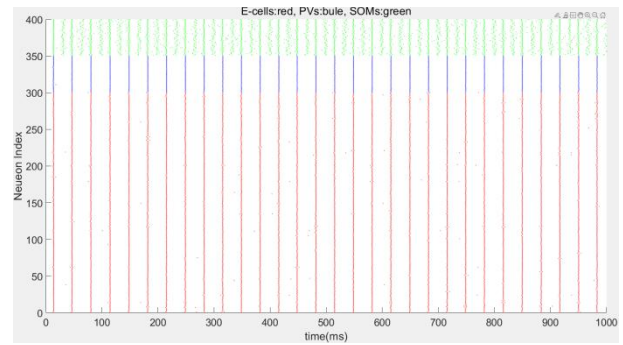
Fig. 23. Simulation results with different S_{es} . Both projection probability and synaptic strength come from [Chaos'2023]. Refractory period = 3 ms, τ_{delay} = 5 ms.

We can see from above results that the stronger the synaptic couplings from SOMs to PCs, the lower the firing rates of PCs. This observation adhere to our intuition, because the stronger S_{es} means it will take longer time for PCs to recover from the inhibition from SOMs. When S_{es} exceeds a certain value, PCs receive too strong inhibition to recover from this, thus making the entire network shut down (**Fig. 23. h**). This observation is an indication that we can adjust the overall excitation within the network by tuning the S_{es} , and that the shut down of the brain maybe caused by the unbalanced Excitation/Inhibition in the cortex (e.g., a short period of unconsciousness after the seizure of epilepsy).


 (e) $S_{es} = 0.0282$

 (f) $S_{es} = 0.0295$

 (a) $S_{is} = 0.00$ (i.e., SOMs are not involved in inhibiting PVs)



(b) $S_{is} = 0.0245$ (original data from [Chaos'2023])



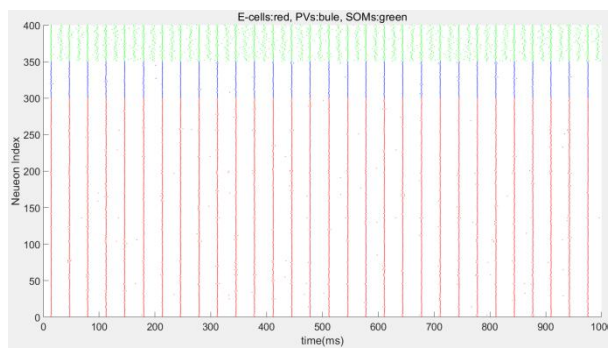
(f) $S_{is} = 0.0295$

Fig. 24. Simulation results with different S_{is} . Both projection probability and synaptic strength come from [Chaos'2023]. Refractory period = 3 ms, $\tau_{delay} = 5$ ms.

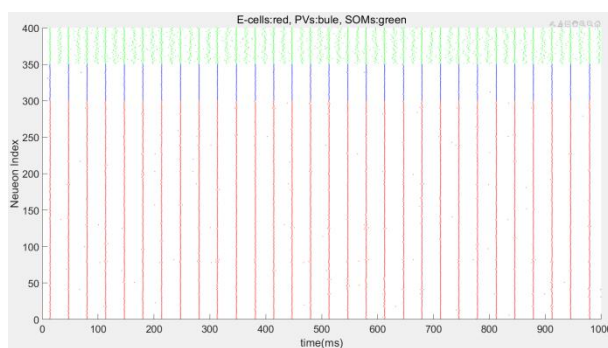
From above results we can see that the synaptic strength from SOMs to PVs has much less effect on the network dynamics than S_{es} , which indirectly emphasize the importance of S_{es} .

I also conducted simulations of scanning S_{es} and S_{ei} with finer grain, you can find them in *Week6.pptx*.

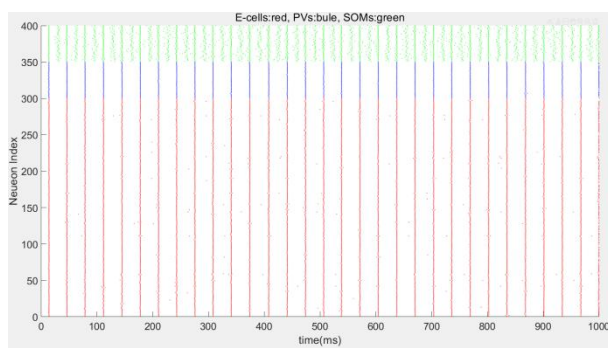
Next I swept the time delay of dendritic inhibition from SOM interneurons again, but this time I conducted two-dimensional parameter scanning of τ_{es}^{delay} and τ_{is}^{delay} , instead of considering them as the same value. And this time you can find the values of these two parameters in the title of each figure below, and I also provided the firing rate data on the bottom right of them.



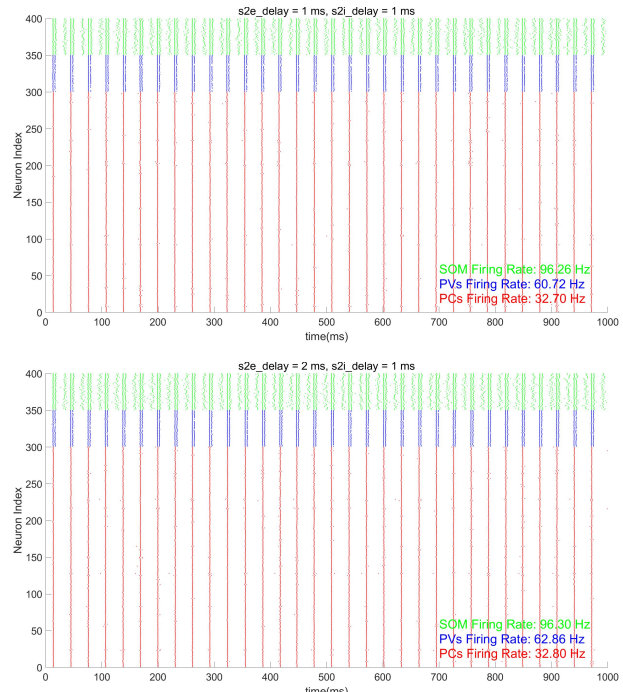
(c) $S_{is} = 0.0258$



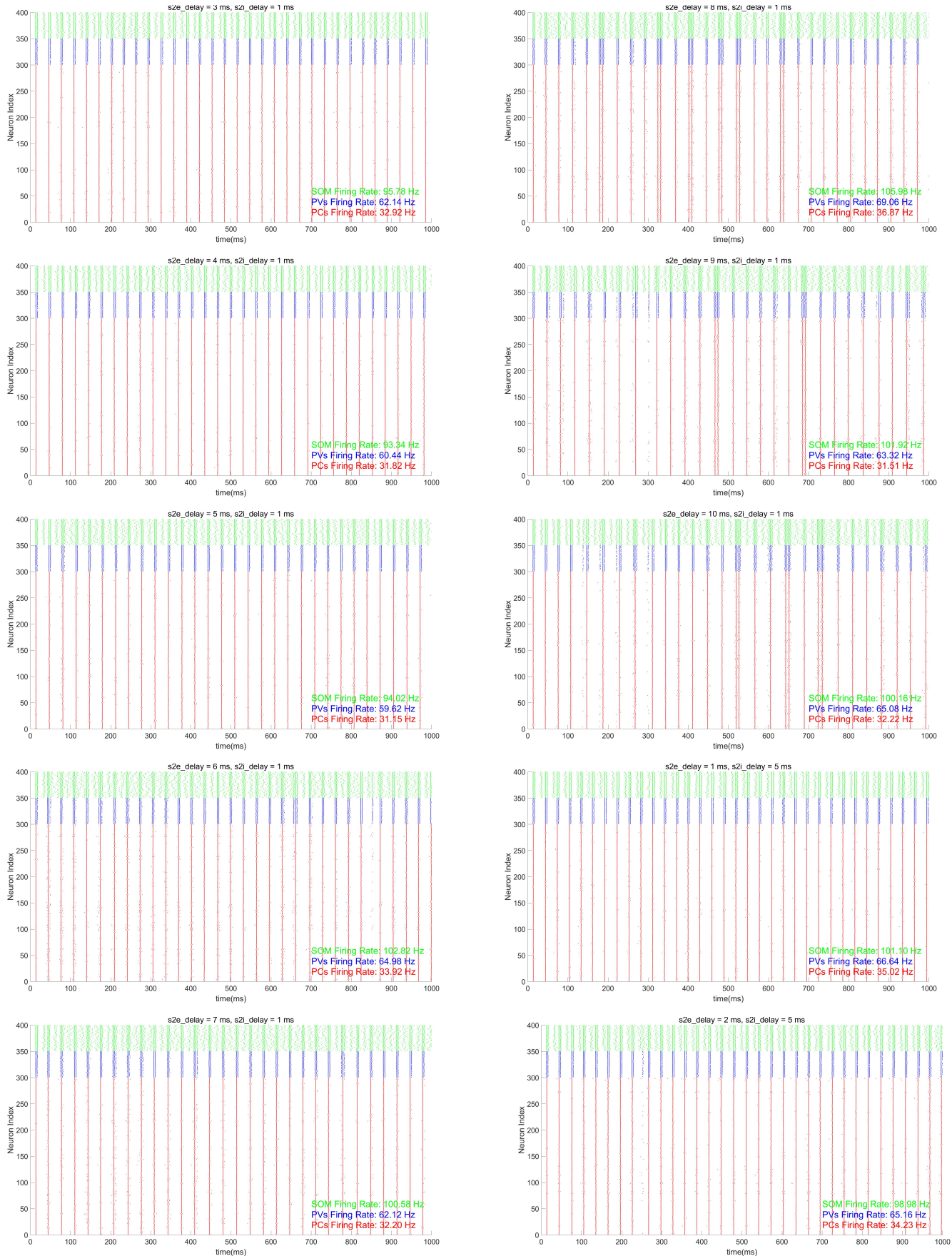
(d) $S_{is} = 0.0270$



(e) $S_{is} = 0.0282$



Research Document: Neuronal Synchronization and Oscillations



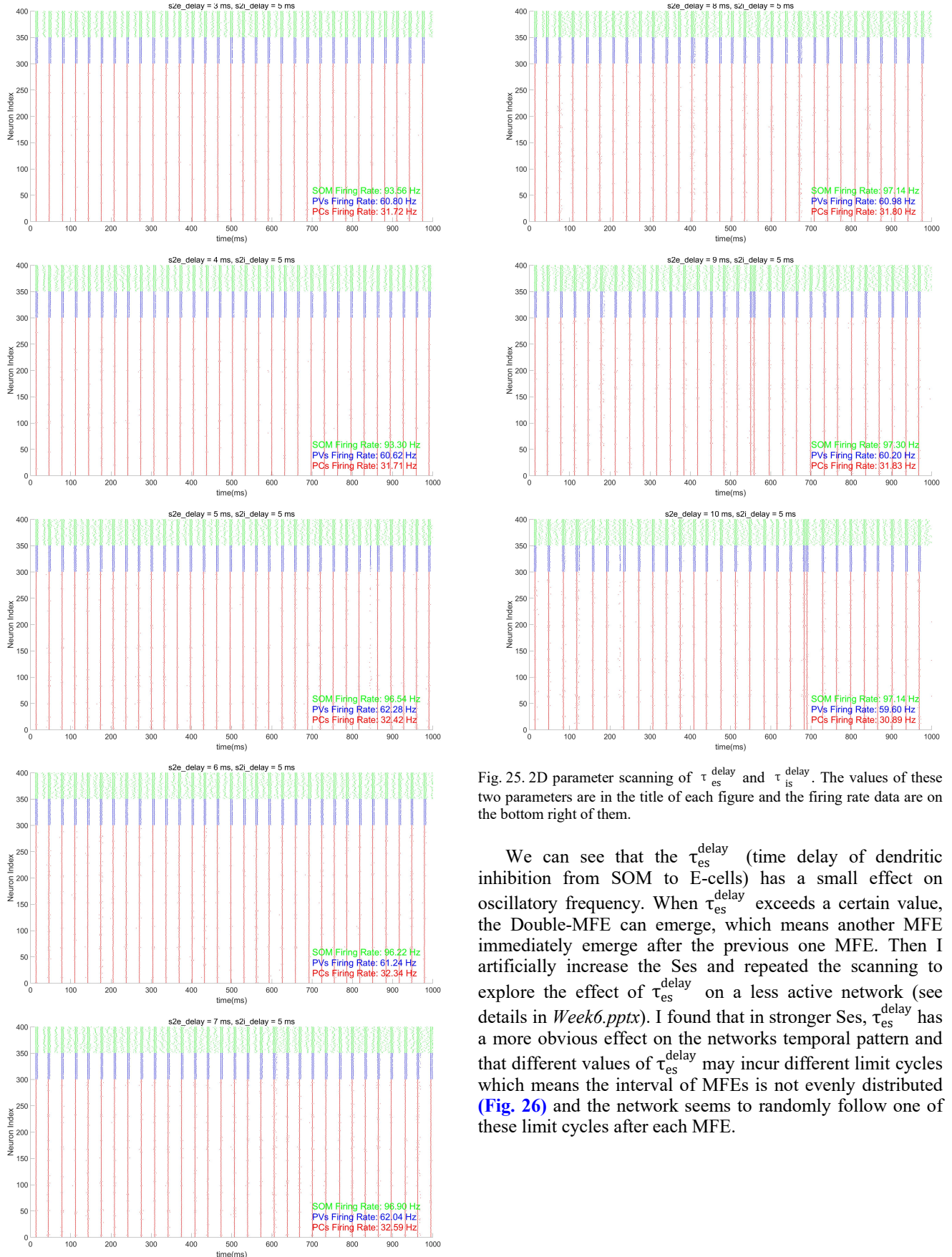


Fig. 25. 2D parameter scanning of τ_{es}^{delay} and τ_{is}^{delay} . The values of these two parameters are in the title of each figure and the firing rate data are on the bottom right of them.

We can see that the τ_{es}^{delay} (time delay of dendritic inhibition from SOM to E-cells) has a small effect on oscillatory frequency. When τ_{es}^{delay} exceeds a certain value, the Double-MFE can emerge, which means another MFE immediately emerge after the previous one MFE. Then I artificially increase the Ses and repeated the scanning to explore the effect of τ_{es}^{delay} on a less active network (see details in Week6.pptx). I found that in stronger Ses, τ_{es}^{delay} has a more obvious effect on the networks temporal pattern and that different values of τ_{es}^{delay} may incur different limit cycles which means the interval of MFEs is not evenly distributed (Fig. 26) and the network seems to randomly follow one of these limit cycles after each MFE.

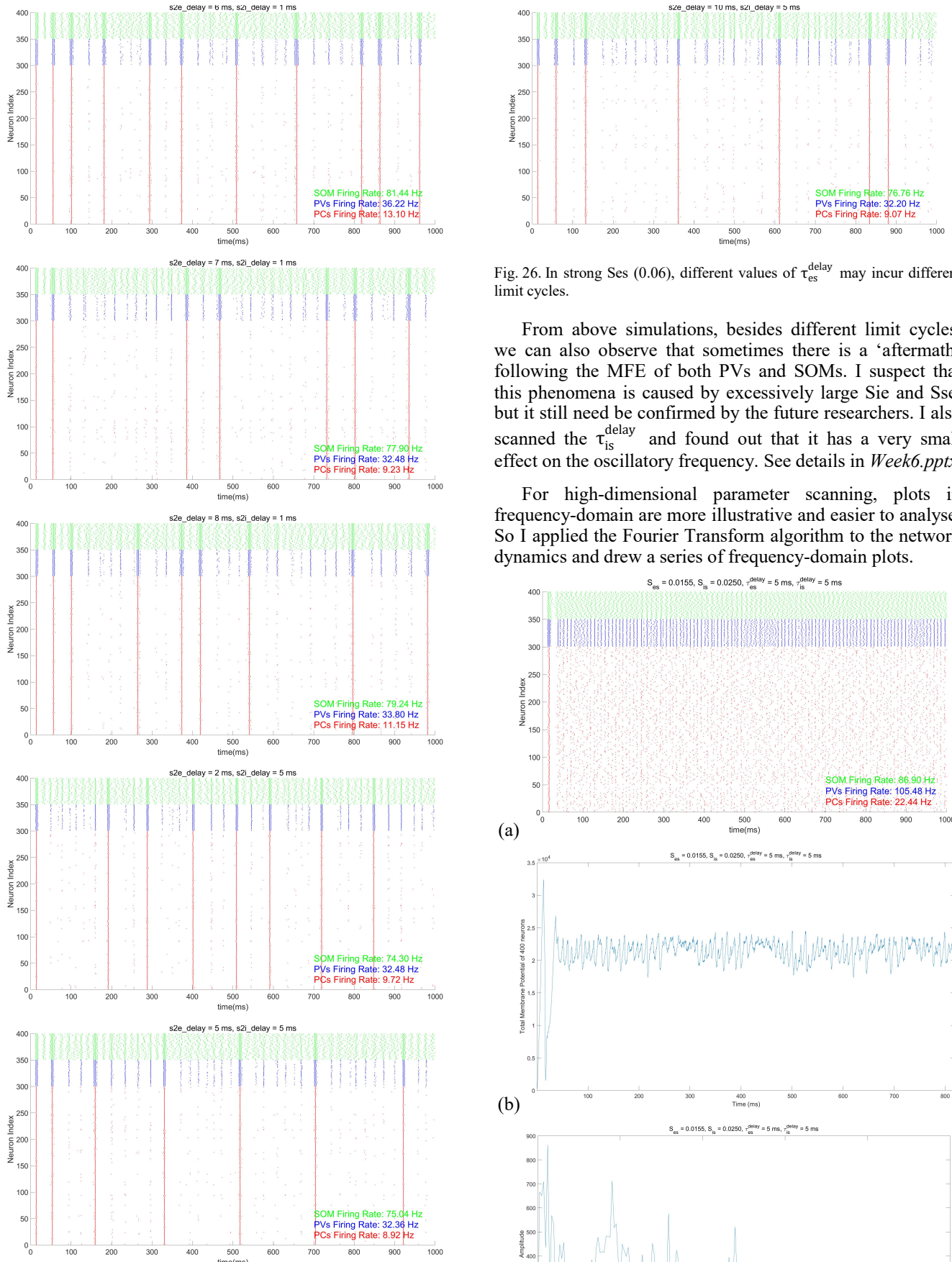
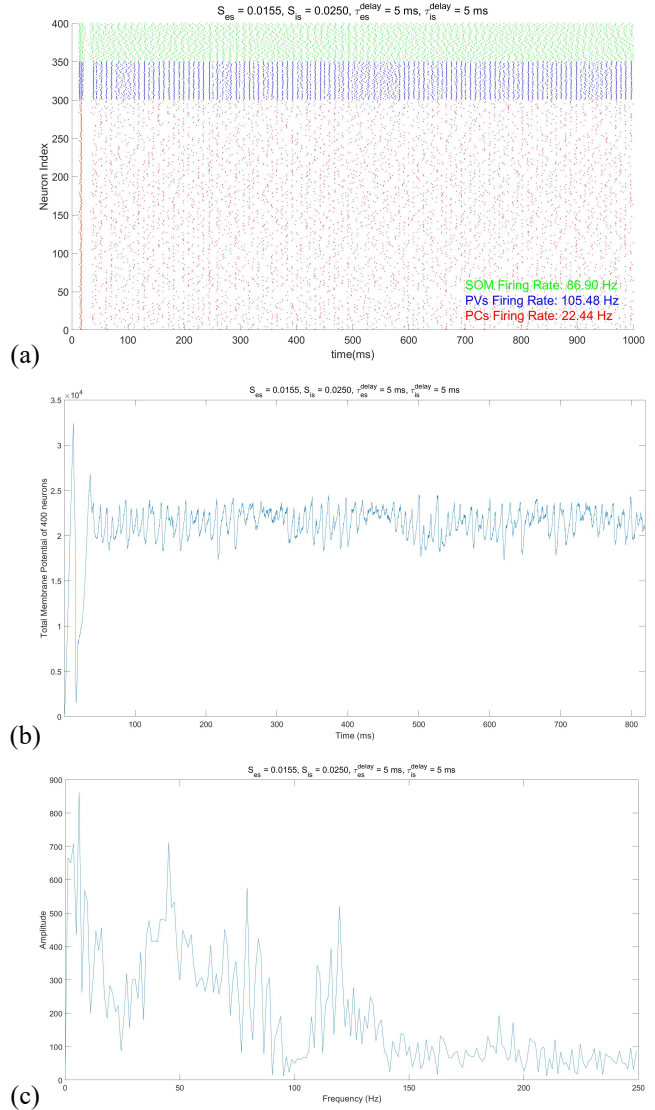


Fig. 26. In strong Ses (0.06), different values of τ_{es}^{delay} may incur different limit cycles.

From above simulations, besides different limit cycles, we can also observe that sometimes there is a ‘aftermath’ following the MFE of both PVs and SOMs. I suspect that this phenomena is caused by excessively large Sie and Sse, but it still need be confirmed by the future researchers. I also scanned the τ_{is}^{delay} and found out that it has a very small effect on the oscillatory frequency. See details in Week6.pptx.

For high-dimensional parameter scanning, plots in frequency-domain are more illustrative and easier to analyse. So I applied the Fourier Transform algorithm to the network dynamics and drew a series of frequency-domain plots.



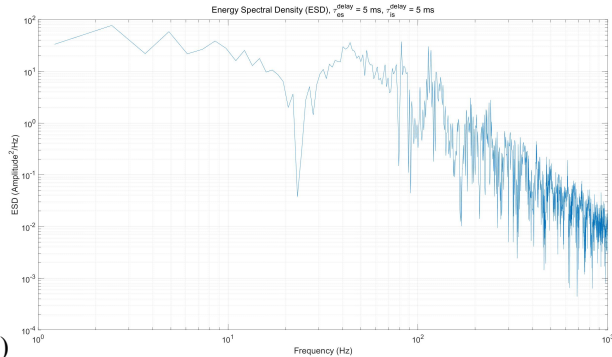
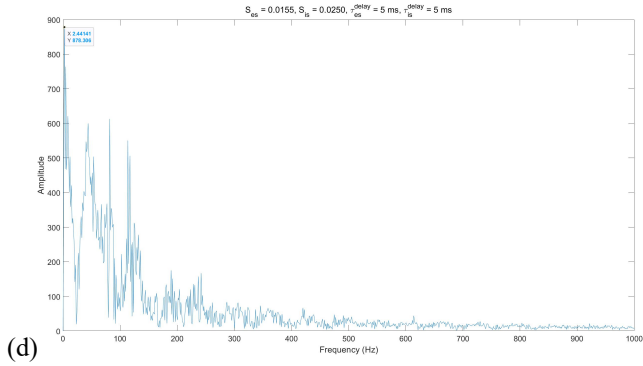


Fig. 27. Frequency-domain figures of network dynamics. (a) Temporal pattern, with projection probability and synaptic strength from the Allen Institute original data. (b) The total membrane potentials of all of the 400 neurons in the network. (c) FFT of the total membrane potentials. (d) FFT result in larger frequency range. (e) Energy Spectral Density.

From frequency-domain plots, we can clearly observe the dominant oscillatory frequency. In the simulation results shown in Fig. 27, I chose to use the original projection probability and synaptic strength data from Allen institute. In Fig. 27C, we can see multiple frequency peaks in the figure, which reflects the various timescales of interplay contained in the network.

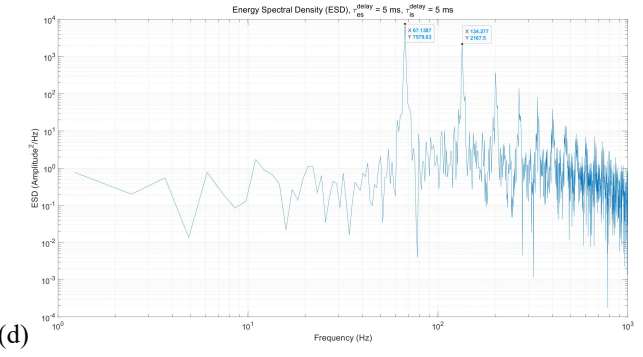
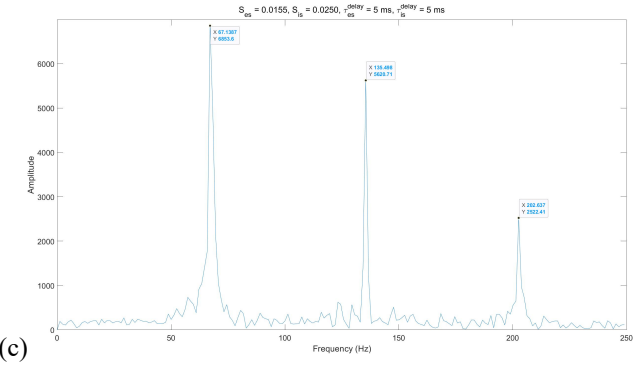
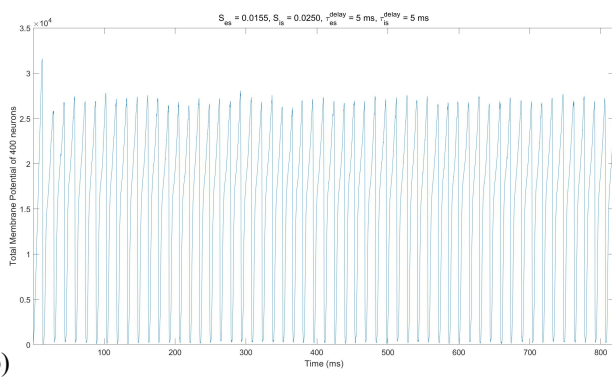
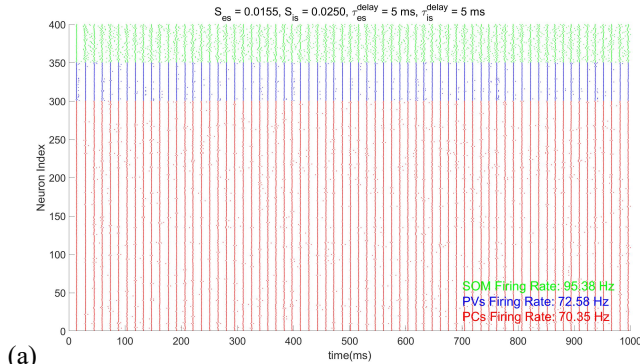


Fig. 28. Frequency-domain figures of network dynamics based on Allen Institute data, with adjusted P_{ee} and P_{ie} .

In order to get a more clear firing pattern in time-domain, I artificially adjusted the P_{ee} (from 0.533 to 0.160) and P_{ie} (from 0.220 to 0.395) and got the results shown in Fig. 28, where we can see one obvious dominant frequency (the other two peaks are caused by frequency doubling and serve no purpose).

Based on the adjusted data set and with the help of Fourier Transform algorithm, we are able to draw the following intuitive figures.

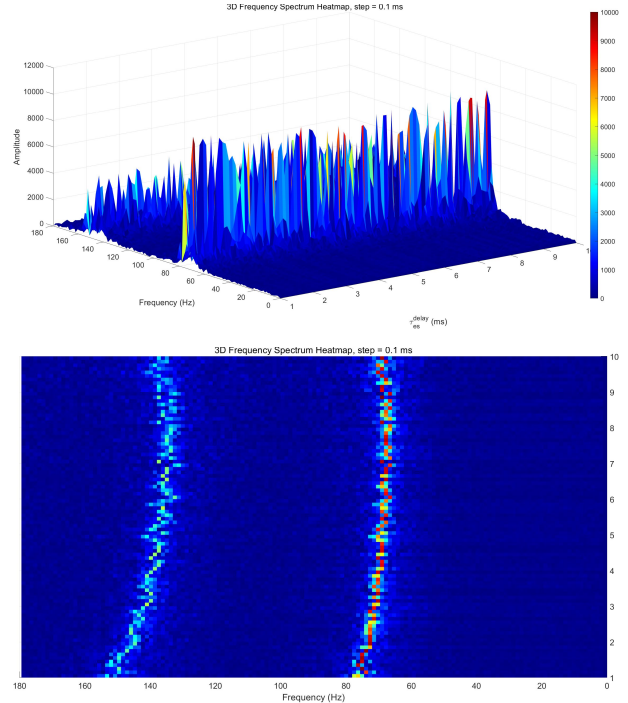


Fig. 29. 3D frequency spectrum heat-map for scanning τ_{es}^{delay} and its bird view.

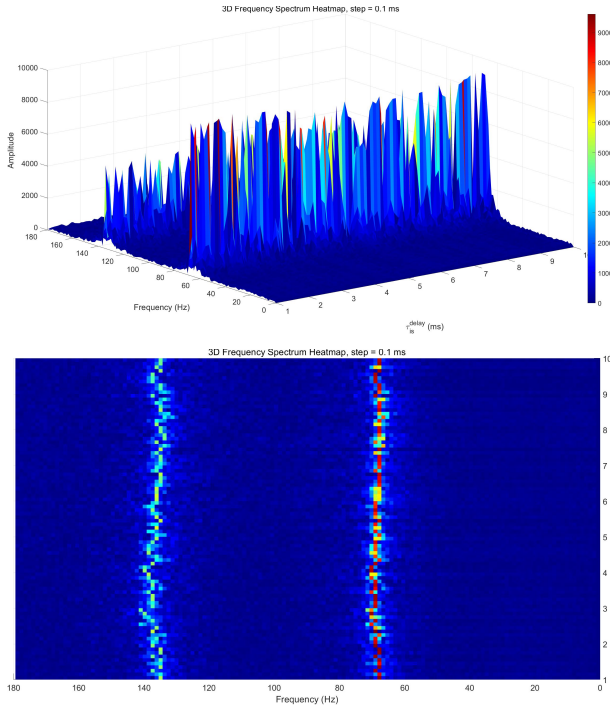


Fig. 30. 3D frequency spectrum heat-map for scanning τ_{is}^{delay} and its bird view.

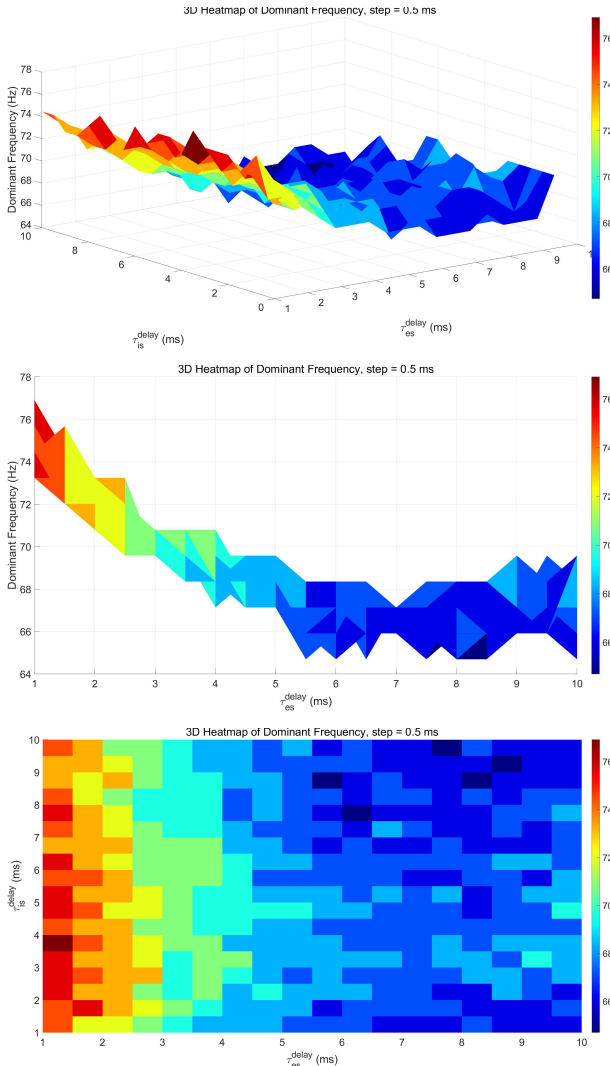


Fig. 31. Dominant frequency map for 2D parameter scanning of τ_{es}^{delay} and τ_{is}^{delay} , with its side view and bird view provided.

The above frequency-domain figures can further confirm our previous conclusions obtained from the analysis of temporal pattern. For example, the declining slope shown in the side view of Fig. 31 reveals that the dominant oscillatory frequency will decrease with the increasing τ_{es}^{delay} .

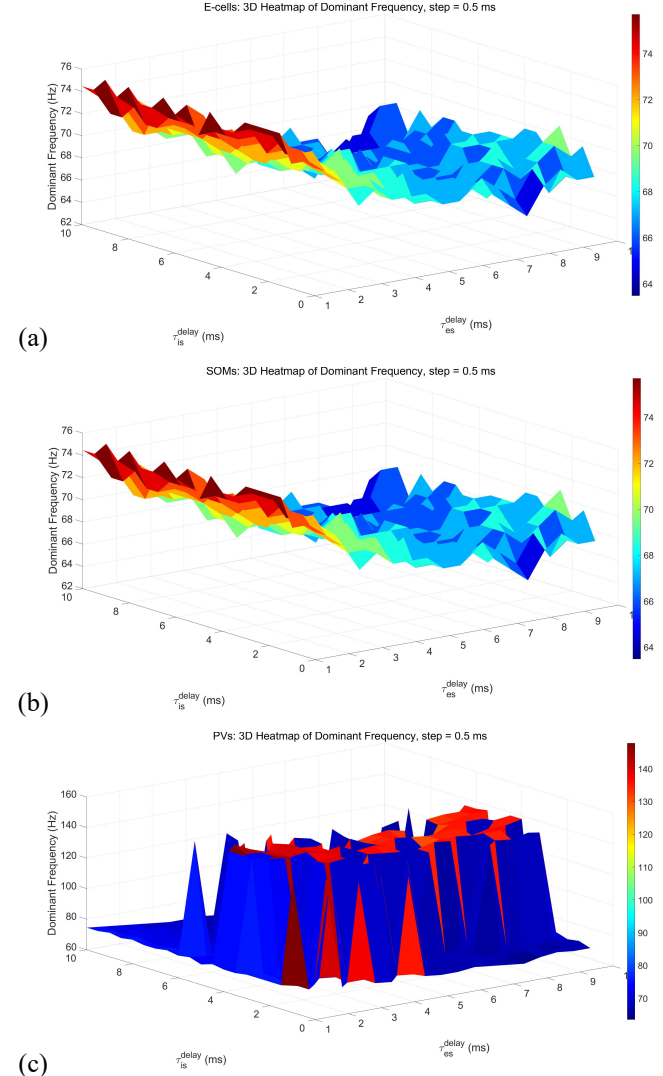


Fig. 32. 3D heat-map of dominant frequency for (a) PCs, (b) SOMs and (c) PVs, respectively.

An interesting finding is that the dominant frequency heat-map for PCs and SOMs are roughly the same (Fig. 32. A&B) and they correspond to the heat-map of the whole network shown in Fig. 31A. While the heat-map of PVs is largely different, and it probably reveals that PVs account for the high-frequency component in the network.

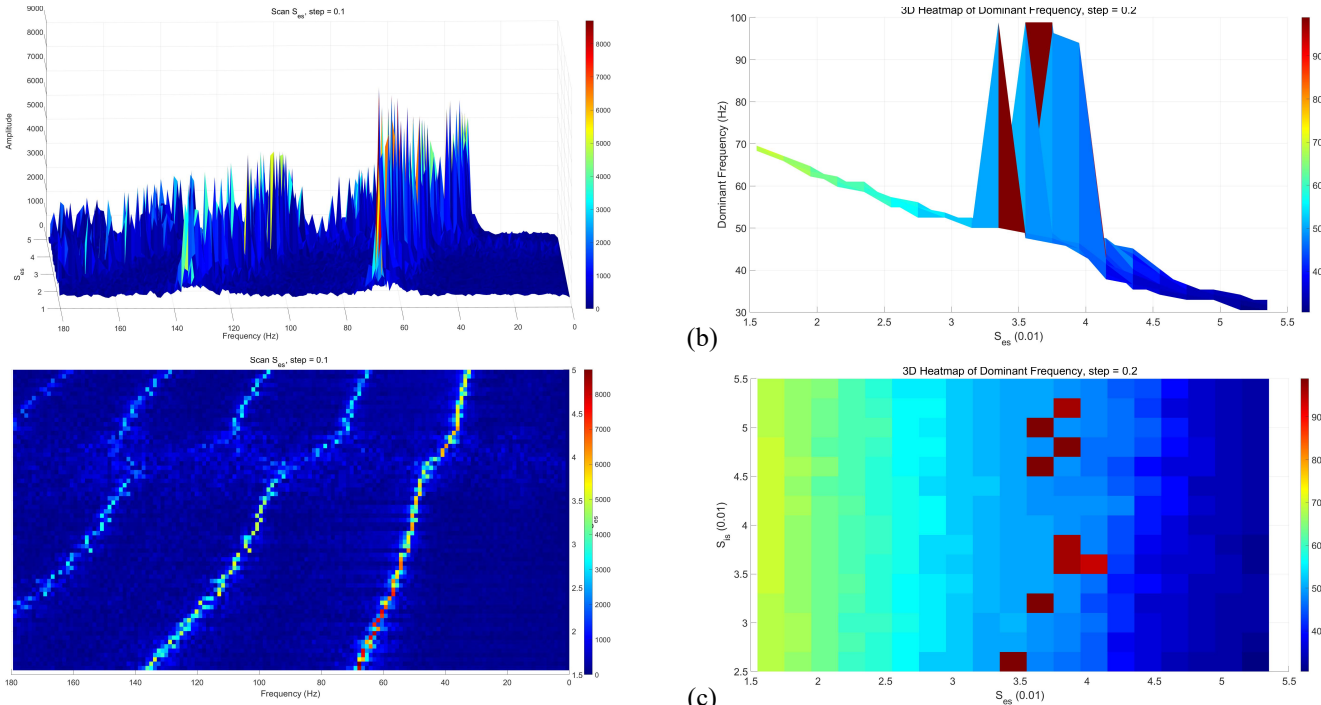


Fig. 33. 3D frequency spectrum heat-map for scanning Ses and its bird view.

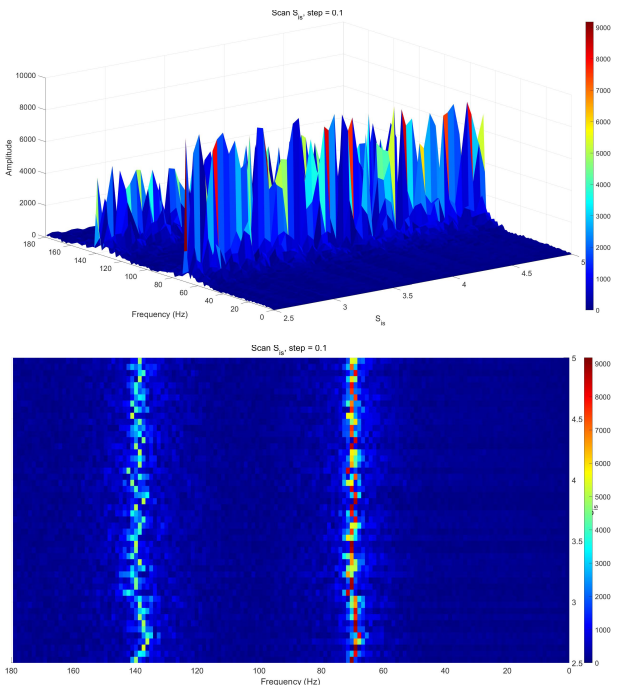


Fig. 34. 3D frequency spectrum heat-map for scanning Sis and its bird view.

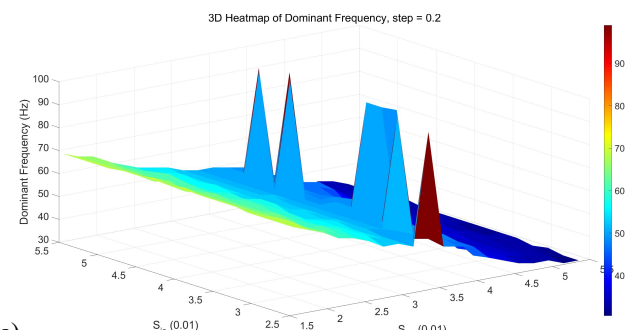
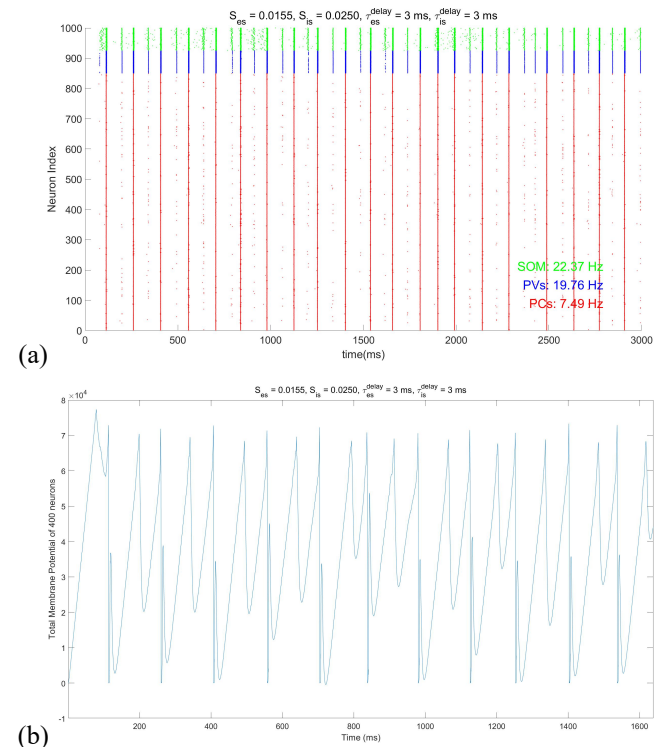


Fig. 35. Dominant frequency map for 2D parameter scanning of Ses and Sis, with its side view and bird view provided.

Fig. 33, 34, 35 present the frequency-domain figures of scanning Ses and Sis, which also clearly prove the correctness of our previous conclusions. The declining slope shown in the Fig. 35B directly reflect the effect of synaptic strength from SOM interneurons to pyramidal neurons on decreasing the oscillatory frequency.



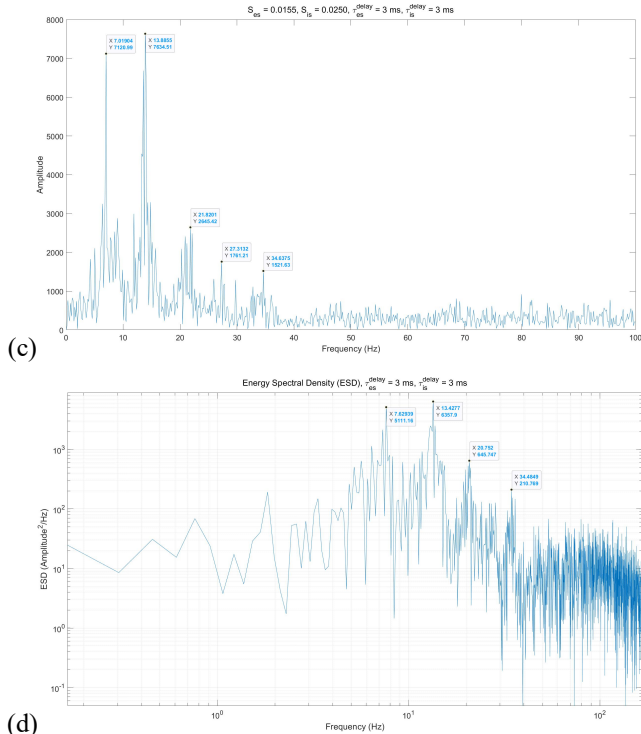


Fig. 36. Frequency-domain figures of the small copy of the network in Allen Institute, which consist of 1000 neurons.

As above mentioned, I tried to built a small copy of the network in Allen Institute in the late stage of this project. In this network, I determined the projection probability to ensure the average number of connections of one neuron is kept in line with that in the Allen Institute network, using the estimation model described in part II.D. **Fig. 36** shows the basic frequency-domain figures of this network, and the following parameter scanning work need to be done by the future researchers.

V. FUTURE RESEARCH

A. NYUSH - Software Simulation

I have established the basic framework of the network, set up frequency-domain analysis, and summarized the core design methods in this document. However, there is still significant work needed to fully achieve the project's objectives. Future tasks include, but are not limited to:

1. Improving the estimation model for calculating the average number of connections for specific neurons to obtain more accurate projection probability data.
2. Finding a more suitable method to translate the synaptic strength data from the Allen Institute before applying it to our network, given that our neuron model is much simpler and differs significantly from theirs.
3. Carefully selecting the parameters for the refractory period, dendritic inhibition time delay, and external Poisson input frequency through extensive investigations.
4. Introducing VIP interneurons into the network and incorporating Spike-Frequency Adaptation in SOM and VIP interneurons to reproduce slow-band neuronal oscillations.

B. HUST - Hardware Implementation

The Allen Institute for Brain Science has developed data-driven models of the mouse primary visual cortex (area V1),

integrating findings from extensive literature and high-throughput experimental pipelines. These models are constructed at two levels of granularity, using either biophysically detailed neuron models or Generalized Leaky Integrate-and-Fire (GLIF) point-neuron models. I believe the Allen Institute's mouse visual cortex model is a good reference for our work. We can apply the dual-mode neuron model we've developed to create a small-scale version of their network, facilitating switching between coarse-grained and fine-grained analyses.

We could build a network consisting of 400 dual-mode neurons, capable of switching between 400 Hodgkin-Huxley (HH) neurons and 1200 Adaptive Exponential (AdEx) neurons. This would allow for analysis of the network across different levels of biological granularity.

Before building the network, we need to modify the dual-mode neuron model to support this switch. Specifically, we need to enable our dual-mode neuron model to switch from one HH neuron to three AdEx neurons. I already have a solution in mind. Our current dual-mode neuron model includes three RFC-CORDIC modules, one adder, and one multiplier. To accommodate three AdEx neurons, we would need to add two more adders and two multipliers. Then, we would adjust the pipeline scheduling diagram to fully utilize these components for a single membrane potential update in the HH neuron.

Since three multipliers will be available for each HH neuron, we can eliminate the need for the CORDIC module to handle the integer part of the exponential calculations—this step largely reduces accuracy and increases computation latency in the RFC-CORDIC module. By doing so, we can expect further improvements in both accuracy and latency of our model.

By constructing this network and observing oscillatory patterns under different configurations, we can demonstrate the effectiveness of our dual-mode neuron model.

SUMMARY AND ACKNOWLEDGMENT

For the first time in my life, I was able to fully immerse myself in research without any distractions, and for that, I am deeply grateful to Prof. Xiao and NYUSH for providing me with such a valuable and memorable experience.

As I reflect on my research journey at NYUSH, there are two dominant motivations consistently driving me forward. The first is my fascination with the brain. I've always been curious about how the brain works and what processes unfold within it. The second is my passion for engineering, especially the thrill of recreating brain functions, whether through software simulations or hardware implementations. I will never forget the excitement I felt when my network code ran successfully, producing meaningful results. This experience has not only strengthened my determination to pursue Neuromorphic Engineering, but also solidified my academic aspiration to replicate the brain on a silicon chip.

Thank you, Prof. Xiao, for your unwavering and meticulous guidance. I am also grateful to Qingyu, Tim, and Zhongyi for your support and companionship, and to Eva Kang, Rona, and Jiaying Wu for making my daily life at NYUSH so much easier. It is because of all of you that my time at NYUSH has been so memorable and wonderful.

I also want to thank my teachers at HUST, Prof. Chao Wang and Prof. Guoqiang Ren, for recommending me for this project, and my dear Gaogao for providing me with constant spiritual encouragement during my stay in Shanghai.

To NYUSH, our story comes to an end here. I hope fate will bring us together again someday.s

REFERENCES

- [1] **[Neuron'1996]** Miles, Richard, et al. "Differences between somatic and dendritic inhibition in the hippocampus." *Neuron* 16.4 (1996): 815-823.
- [2] **[T Neuro.'1997]** Stuart, Greg, et al. "Action potential initiation and backpropagation in neurons of the mammalian CNS." *Trends in neurosciences* 20.3 (1997): 125-131.
- [3] **[Science'2004]** Buzsaki, György, and Andreas Draguhn. "Neuronal oscillations in cortical networks." *science* 304.5679 (2004): 1926-1929.
- [4] **[J Physio.'2004]** Tiesinga, Paul H., et al. "Inhibitory synchrony as a mechanism for attentional gain modulation." *Journal of Physiology-Paris* 98.4-6 (2004): 296-314.
- [5] **[Annual Rev. Neuro.'2009]** Fries, Pascal. "Neuronal gamma-band synchronization as a fundamental process in cortical computation." *Annual review of neuroscience* 32.1 (2009): 209-224.
- [6] **[Nature Neuro.'2011]** Hofer, Sonja B., et al. "Differential connectivity and response dynamics of excitatory and inhibitory neurons in visual cortex." *Nature neuroscience* 14.8 (2011): 1045-1052.
- [7] **[Dev. Neuro.'2011]** Rudy, B., Fishell, G., Lee, S., & Hjerling-Leffler, J. (2011). Three groups of interneurons account for nearly 100% of neocortical GABAergic neurons. *Developmental Neurobiology*, 71(1), 45-61.
- [8] **[Annual Rev. Neuro.'2012]** Buzsáki, György, and Xiao-Jing Wang. "Mechanisms of gamma oscillations." *Annual review of neuroscience* 35.1 (2012): 203-225.
- [9] **[J Neuro.'2012]** Levy, Robert B., and Alex D. Reyes. "Spatial profile of excitatory and inhibitory synaptic connectivity in mouse primary auditory cortex." *Journal of Neuroscience* 32.16 (2012): 5609-5619.
- [10] **[J Neuro.'2013]** Cottam, James CH, Spencer L. Smith, and Michael Häusser. "Target-specific effects of somatostatin-expressing interneurons on neocortical visual processing." *Journal of Neuroscience* 33.50 (2013): 19567-19578.
- [11] **[SEI'2013]** Fujino, Yozo, and Dionysius Siringoringo. "Vibration mechanisms and controls of long-span bridges: a review." *Structural Engineering International* 23.3 (2013): 248-268.
- [12] **[J Neurosci'2013]** Hioki, H. et al. Cell type-specific inhibitory inputs to dendritic and somatic compartments of parvalbuminexpressing neocortical interneuron, *J. Neurosci.* 33, 544–555 (2013).
- [13] **[Nature Neuro.'2016]** Morgenstern, Nicolás A., Jacques Bourg, and Leopoldo Petreanu. "Multilaminar networks of cortical neurons integrate common inputs from sensory thalamus." *Nature neuroscience* 19.8 (2016): 1034-1040.
- [14] **[Nature Rev. Neuro'2016]** Urban-Ciecko, Joanna, and Alison L. Barth. "Somatostatin-expressing neurons in cortical networks." *Nature Reviews Neuroscience* 17.7 (2016): 401-409.
- [15] **[Neuron'2016]** Tremblay, R., Lee, S., & Rudy, B. (2016). GABAergic Interneurons in the Neocortex: From Cellular Properties to Circuits. *Neuron*, 91(2), 260-292.
- [16] **[Nature Comm.'2018]** Teeter, Corinne, et al. "Generalized leaky integrate-and-fire models classify multiple neuron types." *Nature communications* 9.1 (2018): 709.
- [17] **[PLOS'2018]** Arkhipov, Anton, et al. "Visual physiology of the layer 4 cortical circuit in silico." *PLoS computational biology* 14.11 (2018): e1006535.
- [18] **[J Math. Bio.'2019]** Li, Yao, Logan Chariker, and Lai-Sang Young. "How well do reduced models capture the dynamics in models of interacting neurons?." *Journal of mathematical biology* 78 (2019): 83-115.
- [19] **[J NeuPhy.'2019]** Keeley, Stephen, et al. "Firing rate models for gamma oscillations." *Journal of neurophysiology* 121.6 (2019): 2181-2190.
- [20] **[PLOS'2019]** Hertag, Loreen, and Henning Sprekeler. "Amplifying the redistribution of somato-dendritic inhibition by the interplay of three interneuron types." *PLoS computational biology* 15.5 (2019): e1006999.
- [21] **[Nature Comm.'2020]** Amsalem, Oren, et al. "An efficient analytical reduction of detailed nonlinear neuron models." *Nature communications* 11.1 (2020): 288.
- [22] **[J Neuro.'2020]** Antonoudiou, Pantelis, et al. "Parvalbumin and somatostatin interneurons contribute to the generation of hippocampal gamma oscillations." *Journal of Neuroscience* 40.40 (2020): 7668-7687.
- [23] **[Neuron'2020]** Billeh, Yazan N., et al. "Systematic integration of structural and functional data into multi-scale models of mouse primary visual cortex." *Neuron* 106.3 (2020): 388-403.
- [24] **[U Arizona'2020]** Xiao, Zhuocheng. *Neuronal Oscillations: In Hippocampal Functions and in Simulations*. Diss. The University of Arizona, 2020.
- [25] **[FNC'2022]** Ibarra-Lecue, Inés, Saskia Haegens, and Alexander Z. Harris. "Breaking down a rhythm: Dissecting the mechanisms underlying task-related neural oscillations." *Frontiers in Neural Circuits* 16 (2022): 846905.
- [26] **[eNeuron'2022]** Fernandez, Fernando R., et al. "Kinetics and connectivity properties of parvalbumin-and somatostatin-positive inhibition in layer 2/3 medial entorhinal cortex." *eneuro* 9.1 (2022).
- [27] **[Chaos'2023]** Wu, Tianyi, et al. "Multi-band oscillations emerge from a simple spiking network." *Chaos: An Interdisciplinary Journal of Nonlinear Science* 33.4 (2023).